FINAL REPORT ~ FHWA-OK-15-03

PROTOTYPE REINFORCED SOIL EMBANKMENT FOR RECONSTRUCTION OF US ROUTE 62 SLOPE FAILURE IN CHICKASHA, OK

Kianoosh Hatami, Ph.D., P.Eng.
Gerald A. Miller, Ph.D., P.E.
Danial Esmaili, Ph.D.
School of Civil Engineering and Environmental Science
College of Engineering
The University of Oklahoma

January 2015

DISCLAIMER

The contents of this report reflect the views of the author(s) who is responsible for the facts and the accuracy of the data presented herein. The contents do not necessarily reflect the views of the Oklahoma Department of Transportation or the Federal Highway Administration. This report does not constitute a standard, specification, or regulation. While trade names may be used in this report, it is not intended as an endorsement of any machine, contractor, process, or product.

PROTOTYPE REINFORCED SOIL EMBANKMENT FOR RECONSTRUCTION OF US ROUTE 62 SLOPE FAILURE IN CHICKASHA, OK

FINAL REPORT ~ FHWA-OK-15-03
ODOT SP&R ITEM NUMBER 2160

Submitted to:

John R. Bowman, P.E.
Director of Capital Programs
Oklahoma Department of Transportation

Submitted by:

Kianoosh Hatami, Ph.D., P.Eng.
Gerald A. Miller, Ph.D., PE
Danial Esmaili, Ph.D
School of Civil Engineering and Environmental Science (CEES)
The University of Oklahoma

Oklahoma Department of Transportation

January 2015

TECHNICAL REPORT DOCUMENTATION PAGE

1. REPORT NO. FHWA-OK-15-03	2. GOVERNMENT ACCESSION NO.	3. RECIPIENT'S CATALOG NO.
4. TITLE AND SUBTITLE **Prototype reinforced soil embankment for reconstruction of US 62 slope failure in Chickasha, OK**		5. REPORT DATE **January 2015**
		6. PERFORMING ORGANIZATION CODE
7. AUTHOR(S): **Kianoosh Hatami, Gerald A. Miller and Danial Esmaili**		8. PERFORMING ORGANIZATION REPORT
9. PERFORMING ORGANIZATION NAME AND ADDRESS **School of Civil Engineering and Environmental Science, University of Oklahoma, Norman, OK**		10. WORK UNIT NO.
		11. CONTRACT OR GRANT NO. **ODOT SP&R Item Number 2160**
12. SPONSORING AGENCY NAME AND ADDRESS **Oklahoma Department of Transportation Materials and Research Division 200 N.E. 21st Street, Room 3A7 Oklahoma City, OK 73105**		13. TYPE OF REPORT AND PERIOD COVERED **Final Report** **October 2012- December 2014**
		14. SPONSORING AGENCY CODE
15. SUPPLEMENTARY NOTES		

16. ABSTRACT: One of the main concerns in internal stability of reinforced soil structures constructed with fine-grained or marginal quality soils is the change in shear strength of the soil-reinforcement interface when the soil gravimetric water content (GWC) increases. This increase can occur during construction or service life of the structure, e.g. due to prolonged precipitation. The resulting loss in the soil matric suction could reduce the interface shear strength leading to serviceability problems or even failure of the reinforced soil structure. In this study, three (3) 1 m-high and two (2) 1.7 m-high model embankments were constructed, which were all subjected to strip footing loading in plane-strain condition. The model embankments were constructed using a mixture of lean clay (CL), sand and a small percentage of commercially available sodium bentonite at the GWC values ranging between OMC-2% and OMC+2% (OMC: Optimum Moisture Content). The purpose for building smaller embankment models was to study the behavior of a single soil-geotextile interface in an embankment configuration. Therefore, the smaller models included only a single reinforcement layer which was placed 180 mm below the embankment surface. In contrast, the larger models were intended to simulate field reinforced embankments. Hence, those models were reinforced with four (4) layers of reinforcement with a uniform vertical spacing of 300 mm. The location of single reinforcement layer in smaller models was selected based on preliminary embankment tests and numerical simulations to ensure that it would intercept the failure surface that developed underneath the strip footing near the embankment slope. The embankments were instrumented to measure the footing load, earth pressure, reinforcement strains and the soil GWC and matric suction values during the tests. A primary objective of the embankment tests was to investigate the influence of the as-compacted GWC value of the soil on the performance of the model embankments and thereby, validate or make necessary adjustments in the values of the moisture reduction factors (MRF) for reinforced embankment design that the authors had developed based on their prior pullout and interface shear tests.

17. KEY WORDS: Soil slope structures, Slope stability, Unsaturated soils, Marginal soil, Geosynthetics, Moisture reduction factor	18. DISTRIBUTION STATEMENT No restrictions. This publication is available from the Materials and Research Div., Oklahoma DOT.		
19. SECURITY CLASSIF. (OF THIS REPORT) **Unclassified**	20. SECURITY CLASSIF. (OF THIS PAGE) **Unclassified**	21. NO. OF PAGES 84	22. PRICE N/A

SI* (MODERN METRIC) CONVERSION FACTORS

APPROXIMATE CONVERSIONS TO SI UNITS				
SYMBOL	**WHEN YOU KNOW**	**MULTIPLY BY**	**TO FIND**	**SYMBOL**
LENGTH				
in	inches	25.4	millimeters	mm
ft	feet	0.305	meters	m
yd	yards	0.914	meters	m
mi	miles	1.61	kilometers	km
AREA				
in^2	square inches	645.2	square millimeters	mm^2
ft^2	square feet	0.093	square meters	m^2
yd^2	square yard	0.836	square meters	m^2
ac	acres	0.405	hectares	ha
mi^2	square miles	2.59	square kilometers	km^2
VOLUME				
fl oz	fluid ounces	29.57	milliliters	mL
gal	gallons	3.785	liters	L
ft^3	cubic feet	0.028	cubic meters	m^3
yd^3	cubic yards	0.765	cubic meters	m^3
NOTE: volumes greater than 1000 L shall be shown in m^3				
MASS				
oz	ounces	28.35	grams	g
lb	pounds	0.454	kilograms	kg
T	short tons (2000 lb)	0.907	megagrams (or "metric ton")	Mg (or "t")
TEMPERATURE (exact degrees)				
^{o}F	Fahrenheit	5 (F-32)/9 or (F-32)/1.8	Celsius	^{o}C
ILLUMINATION				
fc	foot-candles	10.76	lux	lx
fl	foot-Lamberts	3.426	candela/m^2	cd/m^2
FORCE and PRESSURE or STRESS				
lbf	poundforce	4.45	newtons	N
lbf/in^2	poundforce per square inch	6.89	kilopascals	kPa

APPROXIMATE CONVERSIONS FROM SI UNITS				
SYMBOL	**WHEN YOU KNOW**	**MULTIPLY BY**	**TO FIND**	**SYMBOL**
LENGTH				
mm	millimeters	0.039	inches	in
m	meters	3.28	feet	ft
m	meters	1.09	yards	yd
km	kilometers	0.621	miles	mi
AREA				
mm^2	square millimeters	0.0016	square inches	in^2
m^2	square meters	10.764	square feet	ft^2
m^2	square meters	1.195	square yards	yd^2
ha	hectares	2.47	acres	ac
km^2	square kilometers	0.386	square miles	mi^2
VOLUME				
mL	milliliters	0.034	fluid ounces	fl oz
L	liters	0.264	gallons	gal
m^3	cubic meters	35.314	cubic feet	ft^3
m^3	cubic meters	1.307	cubic yards	yd^3
MASS				
g	grams	0.035	ounces	oz
kg	kilograms	2.202	pounds	lb
Mg (or "t")	megagrams (or "metric ton")	1.103	short tons (2000 lb)	T
TEMPERATURE (exact degrees)				
^{o}C	Celsius	1.8C+32	Fahrenheit	^{o}F
ILLUMINATION				
lx	lux	0.0929	foot-candles	fc
cd/m^2	candela/m^2	0.2919	foot-Lamberts	fl
FORCE and PRESSURE or STRESS				
N	newtons	0.225	poundforce	lbf
kPa	kilopascals	0.145	poundforce per square inch	lbf/in^2

*SI is the symbol for the International System of Units. Appropriate rounding should be made to comply with Section 4 of ASTM E380.

TABLE OF CONTENTS

LIST OF FIGURES

LIST OF TABLES

EXECUTIVE SUMMARY

Oklahoma Department of Transportation (ODOT) and other departments of transportation in the U.S. are continually faced with the persistent problem of landslides and slope failures along highways. Repairs and maintenance work associated with these failures cost these agencies millions of dollars annually. Reinforced soil technology can provide viable solutions to stabilize or reconstruct highway slopes and embankments. However, one concern in internal stability of reinforced marginal soils is the interface strength properties of reinforcement and soil when the soil gravimetric water content (GWC) increases significantly. This increase can occur during construction or due to prolonged precipitation. Wetting-induced reduction in matric suction and loss of shear strength in the soil and soil-reinforcement interface could lead to excessive deformation or complete failure of reinforced soil structures. In spite of such possibilities and actual failure occurrences, current design guidelines and test protocols for reinforced soil slopes (RSS) in North America do not include provisions to account for the reduction in the interface shear strength due to increased gravimetric water content in the soil.

This study is part of a long-term research project sponsored by the ODOT and OkTC which is aimed at developing design guidelines for reinforced soil slopes (RSS) that are constructed with locally available soils in unsaturated conditions and subjected to climatic factors in Oklahoma. The study described in this report involved construction and testing of three reduced-scale (1 m-high) indoor embankments and two (2) larger scale (1.7 m-high) outdoor reinforced soil embankments at OU to study their performance and to determine moisture reduction factors (MRF) in an actual embankment configuration. The MRF values can be used to determine the change in the soil-reinforcement interface shear strength in internal stability analysis of mechanically stabilized earth (MSE) and reinforced soil slopes (RSS) with significant fines content and thereby, make them more accurate and reliable.

1. INTRODUCTION

Landslides and slope failures along highways are a persistent problem across the U.S. Repairs and maintenance work associated with these failures cost national departments of transportation millions of dollars annually. In Oklahoma, many of these failures occur in the eastern and central parts of the state due to higher topography and poor soil types (Hatami et al. 2010a,b; 2011a,b). A recent example of these failures is a landslide on the US Route 62 in Chickasha, Oklahoma. (Figure 1)

Embankment failure

(a)   (b)

Figure 1. Failed slope of a highway embankment in Chickasha, OK

Design guidelines and specifications for Mechanically Stabilized Earth (MSE) structures in North America recommend the use of coarse-grained soils to repair and stabilize highway slopes and embankments (e.g. Elias et al. 2001; Berg et al. 2009). However, since coarse-grained soils are not commonly available in Oklahoma and many other parts of the U.S., depending on the location of the borrow source relative to the project site, the costs of the fill material and its transportation can be prohibitive. In such cases, locally available soils could be considered as alternative construction materials because they would require less fuel consumption and generate less pollution compared to using high-quality offsite soils. It has been estimated that fuel costs constitute about 20% of the total costs for transportation of high-quality soil (Ou et al. 1982). Overall, the use of marginal soils in reinforced soil structures [e.g. mechanically stabilized walls (MSE) and reinforced soil slopes (RSS)] has been shown to reduce the cost of fill material by up to 60% (Keller 1995). However, in order to reinforce embankment structures that are built with marginal soils, it is important to obtain satisfactory soil-reinforcement interface

performance. The performance of marginal soils and their interface with geosynthetic reinforcement can be complex under construction or service loading conditions. Typically, reinforced soil structures are constructed at gravimetric water content (GWC) values near optimum (i.e. Optimum Moisture Content - OMC). However, several factors could cause the fill moisture content to deviate from the target value. Examples include precipitation during construction, groundwater infiltration and development of excess pore water pressure due to compaction. These factors, in addition to seasonal variations of soil water content, can significantly reduce the strength of the soil-reinforcement interface and lead to excessive deformations or failure during construction or service life of the structure. Therefore, reliable design procedures should be able to account for the influence of matric suction on the strength of the soil and the soil-geosynthetic interface and the resulting factors of safety against failure. Such design provisions are currently not available for reinforced soil structures involving marginal soils.

2. OBJECTIVE AND SCOPE

The main objective of this project was to extend and validate the moisture reduction factors (MRF) for soil-reinforcement interfaces from pullout and interface shear tests in earlier studies (Hatami et al. 2010a,b; 2011a,b) against the values obtained in actual embankment configurations. The pullout capacity and interface shear strength of reinforcement in a soil mass are important factors in stability analysis and design of reinforced soil structures. For internal stability, pullout resistance of the reinforcement, P_r, and interface shear strength of soil and reinforcement are determined using Equations 1 and 2, respectively:

$$P_r = F^* \alpha \sigma'_v L_e C \tag{1}$$

$$\tau = c_a + \sigma'_v \tan\delta \tag{2}$$

Where $F^*, \alpha, \sigma'_v, L_e, C, \tau, c_a$ and δ are pullout resistance factor, stress distribution correction factor, effective vertical stress at soil-reinforcement interface, reinforcement anchorage length, effective unit perimeter (e.g. $C=2$ for strips, grids and sheets), interface shear strength, interface adhesion and interface friction angle, respectively. The hypothesis of this study is that changes in matric suction and gravimetric water content due to wetting of the soil-reinforcement interface could

3

significantly influence the pullout capacity and interface shear strength of the reinforcement in the soil as determined from Equations 1 and 2. Therefore, a moisture reduction factor, $\mu(\omega)$, is applied in Equations 1 and 2 to account for the variation of gravimetric water content and suction on the unsaturated soil-reinforcement interface strength in the form:

$$P_{r\,OMC+2\%} = [F^* \propto \sigma_v' L_e C]_{OMC-2\%}\, \mu(\omega) \tag{3}$$

$$\tau_{OMC+2\%} = [c_a + \sigma_v' \tan \delta]_{OMC-2\%}\, \mu(\omega) \tag{4}$$

In a recent study by the authors and colleagues (Hatami et al. 2010a,b; 2011a,b), a moisture reduction factor [MRF or $\mu(\omega)$] was developed for two different Oklahoma soils (i.e. Minco silt and Chickasha clay) based on the results of pullout and interface shear tests (IST) in the laboratory. The present study involved construction and testing of three reduced-scale (1 m-high) indoor and two (2) larger-scale (1.7 m-high) outdoor reinforced soil embankment models at OU to extend and validate the MRF values for actual embankment configurations.

3. EXTENDED MOHR-COULOMB FAILURE ENVELOPE

The shear strength of an unsaturated soil can be determined using two stress variables: net normal stress $(\sigma_n - u_a)$ and soil matric suction $(u_a - u_w)$ (Fredlund et al. 1978). The net normal stress is the difference between the total stress and pore air pressure, and the matric suction is the difference between the pore air and the pore water pressures. Miller and Hamid (2005) proposed the following equation to determine the shear strength of unsaturated soil-structure interfaces:

$$\tau_s = C_a' + (\sigma_n - u_a) \tan \delta' + (u_a - u_w) \tan \delta^b \tag{5}$$

Where:

C_a': Adhesion intercept

σ_n: Normal stress on the interface

u_a: Pore air pressure

δ': Angle of friction between soil and reinforcement with respect to $(\sigma_n - u_a)$

u_w: Pore water pressure

δ^b: Angle of friction between soil and reinforcement with respect to suction $(u_a - u_w)$

In the case of an unsaturated soil, Mohr's circles representing failure conditions correspond to a 3D failure envelope, where the shear stress (τ) is the ordinate and the two stress variables are the abscissas $(\sigma_n - u_a)$ and $(u_a - u_w)$. The locations of the Mohr's circles in the third dimension are functions of matric suction $(u_a - u_w)$. The planar surface formed by these two stress variables is called the extended Mohr-Coulomb failure envelope.

4. RELATED PREVIOUS STUDIES

A survey of literature related to reinforced soil embankments, walls and foundations that was carried out during the course of this study is summarized in this section.

Bathurst et al. (2003) studied the performance of reinforced and unreinforced slopes under a strip footing load. Their study showed that an increase in the reinforcement length and stiffness increased the ultimate load capacity of the strip footing. Their results also indicated that the bearing capacity of the reinforced embankment was up to two times as large as that of an otherwise identical unreinforced embankment.

Zhang et al. (2003) evaluated the effect of synthetic fibers and non-woven geotextile reinforcements on the stability of clay embankments. Their results showed that every unit increase in the moisture content led to a 3% decrease in the shear strength of the reinforced soil. The study concluded that fiber reinforcement could compensate for the loss of soil shear strength caused by increases in the soil moisture content. The results also indicated that repairing failed slopes with the nonwoven geotextile can decrease repetitive surface failures in slopes of highly plastic soils.

Bueno et al. (2005) studied the field performance of retaining walls reinforced with non-woven geotextiles. A series of nonwoven geotextile-reinforced soil structures was built and instrumented to measure facing displacement, vertical settlement of backfill and reinforcement strain. Their study also showed that the Finite Element Method could be a useful tool to predict the response of geosynthetic-reinforced structures.

Zhan et al. (2006) studied the effect of rainfall infiltration on soil-water interaction in an unsaturated expansive soil slope. Tensiometers, thermal conductivity sensors, vibrating wire earth pressure cells and inclinometers were used to measure the soil matric suction, water content, earth pressure and deformations of the slope. ThetaProbe is an in-situ sensor which measures the volumetric moisture content of the soil by measuring its dielectric constant. The measured changes are converted to a millivolt signal which is proportional to the soil moisture content (or GWC). Zhan et al.'s results indicated that the horizontal displacement and pore water pressure within the slope increased with rainfall. The data showed that the horizontal stress also increased with swelling pressure.

Hossain and Sakai (2007) studied the effect of water content on the behavior of geogrid-reinforced clayey backfill. The tests were performed for moisture contents between 6% and 33% and normal stresses between 48 kPa and 192 kPa. Their results at the moisture content of 32.5% showed that the geogrid pullout strength increased from 75 kPa to 150 kPa by increasing the normal stress from 48 kPa to 192 kPa. Their study also showed that the maximum difference in pullout strength due to difference in water content occurred at the lowest normal stress. The pullout strength at 6.6% water content was 2.3 times as large as the strength at the water content of 32.5%.

Kumar et al. (2007) performed a series of tests on a strip footing rested on reinforced layered sand to determine its ultimate bearing capacity. The foundation consisted of a strong sand layer overlying a low bearing capacity sand deposit. They observed that replacing the top 1B-thick layer of the weak soil (B is the strip footing width) with well graded sand reinforced with 2 to 4 layers of geogrid reinforcement could increase the ultimate bearing capacity of footing up to 4 times and reduced the footing settlement.

Yoo et al. (2007) evaluated the pullout capacity and drainage properties of three types of geosynthetics (i.e. a geogrid, a geotextile and a composite reinforcement) in a weathered granite backfill which contained a significant amount of fines between 25% and 33%. From the results of their pullout tests and finite difference analysis, they concluded that tensile resistance and deformation of the geosynthetic reinforcement was improved when the material included drainage properties, i.e. composite reinforcement was used such as geogrids in combination with geotextiles with good drainage capability.

Bilgin and Kim (2010) investigated the effect of reinforcement length and backfill properties on reinforced soil wall deformations. Their results indicated that the reduction in reinforcement

length from 0.7H to 0.4H (H: height of the wall) could increase the wall deformation by more than 80% and the reinforcement load by up to 20%. Their study also showed that an increase in soil friction angle from 30° to 42° could reduce the maximum wall deformation by up to 50%.

Sawwaf and Nazir (2012) studied the behavior of an eccentrically loaded ring footing on a geogrid-reinforced compacted sand which overlaid loose sand. Their test results showed that the behavior of the ring footing considerably improved as the thickness and relative density of compacted sand layer increased. Their investigation also confirmed that using geosynthetic reinforcement could reduce the required thickness of compacted sand and/or lead to increased bearing capacity of the footing.

Gill et al. (2013) performed a series of large-scale footing tests on geogrid reinforced coal ash slope to study the effects of number of reinforcement layers and the footing setback from the slope crest on load bearing capacity of the slope. Their results showed that increasing the number of reinforcement layers improved the bearing pressure of footing as well as the stiffness of foundation bed. However, the bearing capacity ratio became less significant when the number of geogrids used in the slope exceeded 3. Their data also indicated that the footing setback had a significant effect on the load bearing capacity of unreinforced and reinforced ash slopes. Also, the authors showed that the bearing capacity of footing increased with the footing setback for up to 3B (B: footing width) and beyond that the improvement became insignificant.

Kawamura et al. (2013) constructed a series of small-scale volcanic slopes followed by a large-scale slope (i.e. H: 5 m, W: 2 m and L: 12 m) with the same soil to investigate the failure mechanism and to monitor the slopes performance. Their results indicate that the depth of failed wedge due to rainfall was deeper for a 45°-slope as compared to a 65° slope. It was also observed that the first collapse in both slopes was generated at the toe of slope and afterwards, a second failure was induced with an increase in the water level for each embankment irrespective of its slope angle. The authors also concluded that the evaluation of soil moisture content was important for slope stability analysis in all seasonal conditions.

Keskin and Laman (2013) performed a series of laboratory tests to evaluate the influences of footing setback from the slope crest, slope angle and relative density of sand on the ultimate bearing capacity of strip footings. Their study showed that the ultimate bearing capacity increased with the setback distance and relative density of the sand, but it decreased with the slope angle. Their results also indicated that at a setback distance of 5 times the width of the

footing, the bearing capacity of the footing practically approached that of the same footing on a level ground.

Kim and Lee (2013) studied the effect of rainfall on the stability of unsaturated weathered granite slope in Korea. Results of their analysis indicated that the slope with higher initial suction had greater initial factor of safety and the failure happened later than that with lower initial suction. Their data also confirmed that a slope with higher saturated permeability was more vulnerable to rainfall-induced landslide.

Yoo (2013) performed a numerical investigation on the effect of rainfall on the performance of reinforced soil walls. Their results showed that a geosynthetic reinforced soil wall backfilled with a marginal soil could experience significant deformations and reinforcement loads leading to possible instability. It was observed that the wall displacement increased continuously up to 90 mm at the end of construction at the location of 1/3 H (H: wall height) from the base. It was also observed that the reinforcement load increased during rainfall by as much as 8 KN/m.

Kibria et al. (2014) studied the performance of MSE wall models with a frictional backfill using the Finite Element method. Their results showed that the reinforcement stiffness did not have a noticeable effect in the 4 m-high wall model as compared to the 8 m and 12 m high models. Their data indicated that for length/height ratio L/H = 1, increasing the reinforcement tensile modulus from 250 kN/m to 42000 kN/m reduced the predicted horizontal movement of the wall from 74 mm to 29 mm. Their study also showed that increasing the L/H ratio from 0.5 to 1 resulted in a 70%, 72.5% and 44.2% reduction in horizontal movement of the 12-m, 8-m and 4-m walls, respectively.

Riccio et al. (2014) monitored the performance of a block-faced geogrid wall with a fine-grained backfill. They found that soil compaction resulted in increased reinforcement tension. However, mobilization of friction at the soil-block interface would help reduce the amount of tension that was mobilized in the reinforcement. The data from the inclinometers indicated that lateral movements increased consistently toward the top of the wall and the maximum deflection was 1.5% of the wall height at the end of construction.

Yang et al. (2014) monitored the performance of a 17 m-high, two-tiered geogrid reinforced soil wall which was backfilled with a granular soil-rock mixture after construction. They monitored facing displacement, horizontal earth pressures behind the facing and reinforcement strains in

8

the wall. Their results showed that the large particles in the backfill reduced the bond strength between backfill and the geogrid in localized regions. Their displacement data also indicated that the post-construction displacement of reinforced wall was small (i.e. 0.3% H; H: height of wall) and this lateral movement was due to backfill-reinforcement slippage and time-dependent properties of the soil.

5. EXPERIMENTAL PROGRAM

5.1.　REDUCED-SCALE EMBANKMENT TESTS

The indoor model embankments were constructed using HP570 woven geotextile reinforcement at three different GWC values equal to OMC-2%, OMC and OMC+2% and were subsequently surcharge loaded to failure. The differences in the magnitudes of the soil-geotextile interface strength and soil shear strength among these test cases were used to determine a moisture reduction factor [MRF = $\mu(\omega)$] as per Equation 4 to account for the loss of reinforcement interface shear strength due to increased GWC value in the soil.

5.1.1.　TEST EQUIPMENT

A 2,000 mm (L) × 750 mm (W) × 1,200 mm (H) portable embankment test box with an integrated loading frame was fabricated for the tests carried out in this study (Figure 2). The sidewalls of the test box were lined with 30 mm-thick polycarbonate glass panels so that the embankment deformations (including the formation of the slip plane) could be monitored and measured. The steel columns and the thickness of the polycarbonate glass panels were designed so that the sidewalls of the text box would be essentially rigid when the embankment models were subjected to surcharge loading.
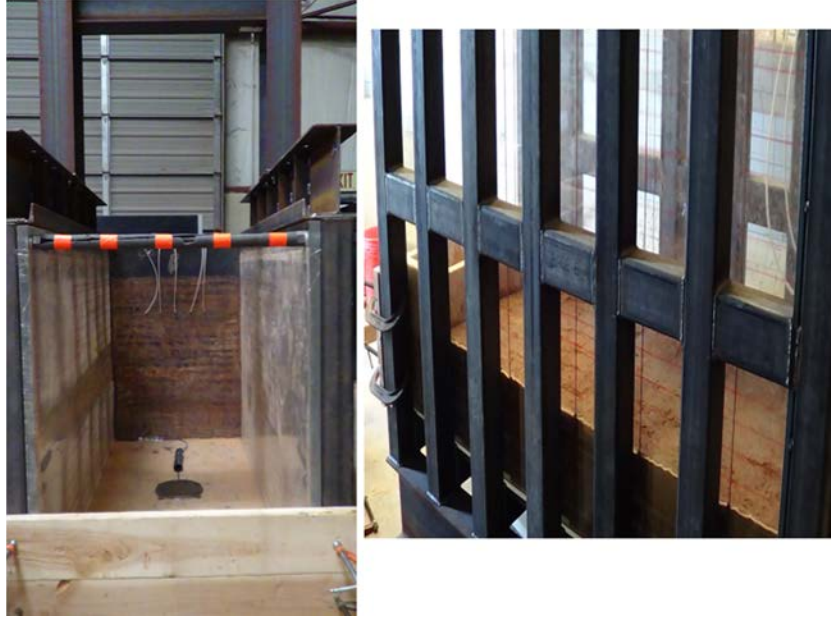
Figure 2. Test box and self-reacting loading frame fabricated for the reduced-scale indoor embankment tests in this study

5.1.2. MATERIAL PROPERTIES

The soil used for the reduced-scale indoor embankment models was a lean clay (called Chickasha clay in this report), i.e. CL and A-6 according to the Unified Soil Classification System (USCS) and AASHTO, respectively with the properties as summarized in Table 1.

Table 1.   Properties of the soil used for reduced-scale indoor embankment tests

Property	CS 2780
Liquid Limit, Plastic Limit (%)	39, 22
Plasticity Index (%)	17
Specific Gravity*	2.75
Sand (%)	4.8
Silt (%) and Clay (%)	69.2, 26
Maximum Dry Unit Weight, kN/m^3 (pcf)	18.8 (120)
Optimum Moisture Content (%)	15

* http://www.eng.utoledo.edu/civil/heydinger/soil%20mechanics/labs/SMSpecGrav.pdf

10

A woven polypropylene (PP) geotextile (Mirafi HP570) was used in the reduced-scale embankment tests carried out in this study. Selected properties of the geotextile are summarized in Table 2.

Table 2. Properties of the woven PP geotextile, Mirafi HP570 that was used for reduced-scale embankment tests carried out in this study

Mechanical and physical properties	ASTM test method	Unit	Maximum average Roll Value HP570
			MD
Tensile strength (at ultimate)	D4595	kN/m (lb/ft)	70 (4800)
Tensile strength (at 5% strength)	D4595	kN/m (lb/ft)	35 (2400)
Factory seam strength	D4884	kN/m (lb/ft)	43.8 (3000)
Permeability	D4491	mm/sec	0.05
Permittivity	D4491	sec^{-1}	0.4
Apparent opening size (AOS)	D4751	mm	0.6
Soil-geotextile interface property			
Interface adhesion at OMC-2%, OMC and OMC+2%	D5321	kPa	13.0, 11.9, 10.1
Interface friction angle at OMC-2%, OMC and OMC+2%	D5321	(°)	13.2, 12.8, 12.4

Further details on the indoor model embankments including soil properties and instrumentation plan are given by Hatami et al. (2013).

5.1.3. TEST PROCEDURE

The silty clay soil (Chickasha clay) was first air dried and broken into small pieces. Afterwards, the soil was passed through a #4 sieve using a shredder and sifter machine (Figure 3). Next, the soil was mixed with water to reach the target GWC value for each test. The wet soil was stored in one hundred and forty (140) 25 kg-buckets and was sealed for at least 24 hours to reach moisture equilibrium. The soil gravimetric water content (GWC) in each bucket was measured using the oven drying method. The above procedure was repeated for every test.

Figure 3.   Processing the soil using a crusher-sifter machine for the reduced-scale indoor embankment tests

5.1.4. CONSTRUCTION OF EMBANKMENT MODELS

Before constructing the model embankments in the test box, its sidewalls were lined with thin clear sheets of Plexiglas to protect the polycarbonate glass panels against scratches during soil placement and compaction. Next, the soil was placed and compacted in the test box in five 100-mm lifts over the lower half of the embankment followed by nine 50-mm lifts. The soil was compacted to 85% and 95% of its maximum dry unit weight (i.e. γ_{dmax} = 18.8 kN/m^3) within the 100-mm lifts (i.e. lower half of the embankment) and 50-mm lifts (upper half), respectively. This was done to expedite the construction of each model embankment given that the focus of the study was on the interface between the single reinforcement layer and the soil within the upper half of each model under the strip footing load (Hatami et al. 2013). It is important to note that the embankments were not meant to be reinforced models. Rather, they provided a single-reinforcement soil mass to produce MRF values for soil-reinforcement shear behavior in an embankment configuration and compare them with those from earlier pullout and interface shear tests. The instrumented geotextile layer was placed at 180 mm from the top of the embankment surface.

12

During construction of each embankment model, the GWC value of each soil lift during compaction was determined by taking six (6) soil samples using the oven drying method (ASTM 2216-10). Additional 3 to 4 random soil samples were also taken after each 2-3 lifts had been compacted to measure their GWC values and ensure that the loss of soil water content as a result of compaction was negligible. Additionally, a total of 12 EC-5 sensors were used to monitor the soil water content in the embankments before and after the tests. However, they were only used at the end of construction to determine when the water content in the embankment stabilized before the embankment could be loaded.

At the end of construction, the test box containing compacted soil at its target gravimetric water content was sealed with plastic sheets at the top for a few days until the moisture and suction sensors inside the embankment reached equilibrium with their surrounding soil. Afterwards, the embankment facing was trimmed to the target slope angle to complete the construction stage before the model was subjected to surcharge loading (Figure 4).

(a)

(b)

Figure 4. (a) Trimming the embankment facing, and (b) Instrumented and complete embankment while surcharge loading

5.1.5. LOADING OF MODEL EMBANKMENTS

The strip footing was placed on the embankment 320 mm away from the embankment crest. A 22-ton, 150-mm stroke hydraulic cylinder (Enerpac Model 506) was used to apply a vertical line load on the model embankments via the strip footing. The vertical load was applied statically in 140 kg increments after it was observed at each load step that the rate of footing settlement had been reduced to less than 0.05 mm/min following the application of the load. Loading continued until a clear and continuous failure surface was observed initiating from the top of the embankment and extending to the embankment facing after being intercepted by the reinforcement layer. After the test was completed and the embankment failed, the test assembly was carefully dismantled.

More details on the test setup, construction and loading of reduced-scale embankment models are provided by Hatami et al. 2013 and 2014, Esmaili 2014 and Chan 2014.

5.1.6. RESULTS

5.1.6.1. SOIL GWC AND SUCTION

Figure 5 shows distributions of the soil GWC within the embankment for all reduced-scale indoor embankment tests that were carried out in this study. The results are compared with the GWC values that were obtained from the SWCC (Hatami et al. 2013) and PST-55 psychrometers to examine the proximity of the as-placed values to the original target values.

(a)

15
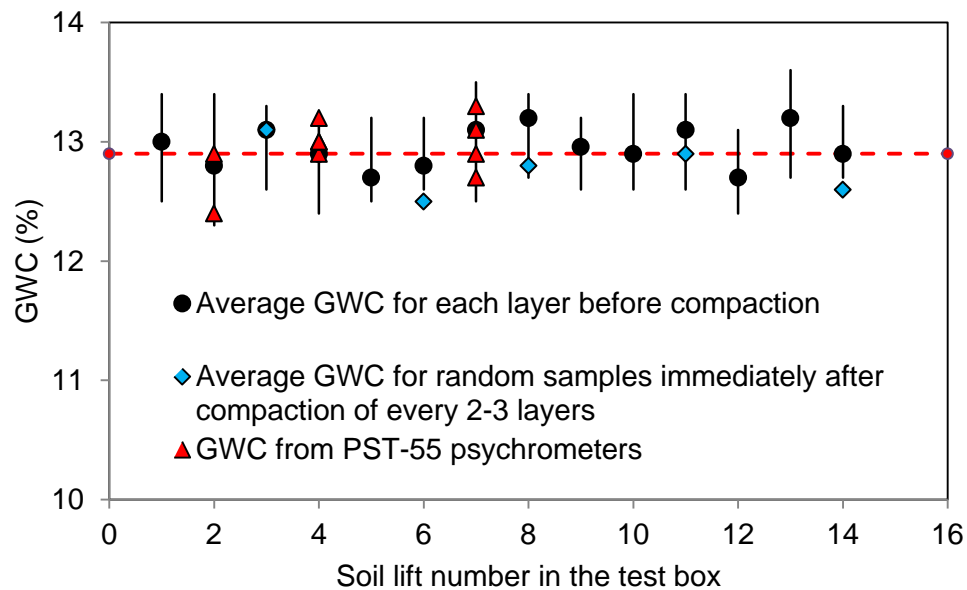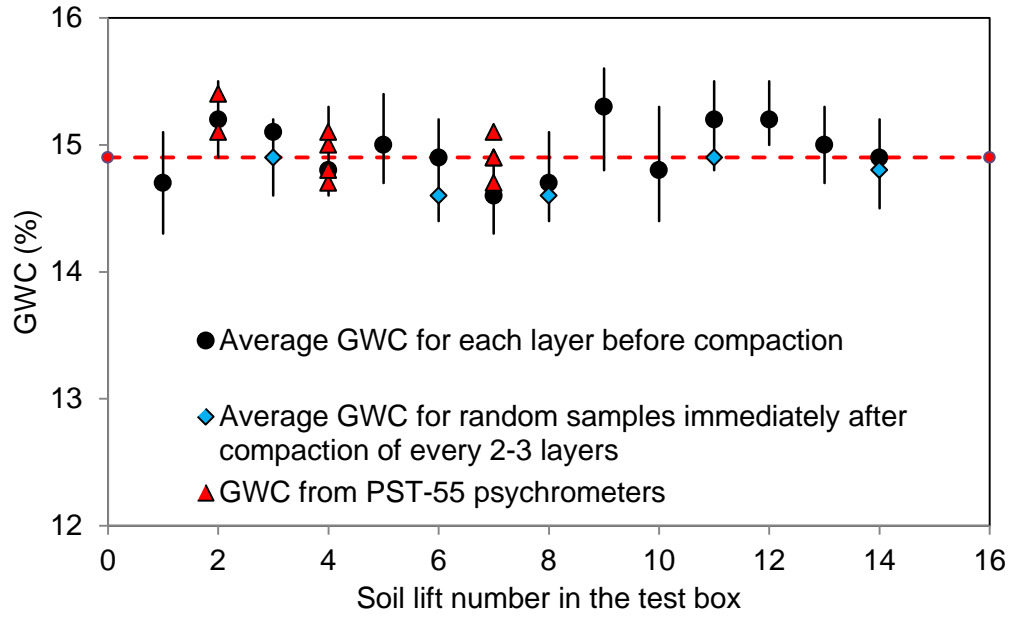
(b)
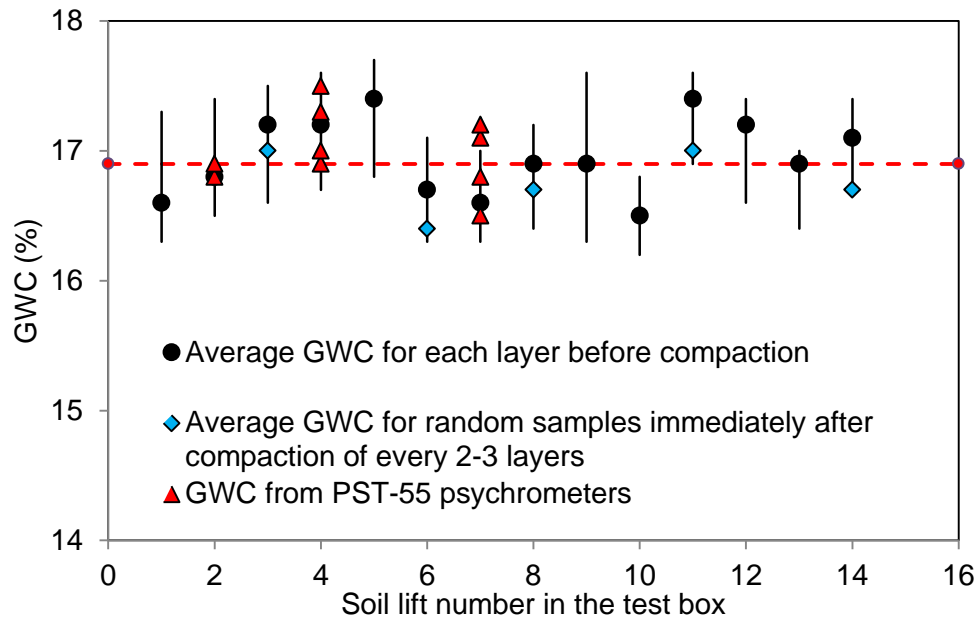
(c)

Figure 5. GWC data within the embankment models constructed with HP570 geotextile reinforcement from oven-drying method and PST-55 psychrometers; (a) Test case at OMC-2%, (b) Test case at OMC and (c) Test case at OMC+2%. Notes: [1] Red dashed line shows the target GWC value, [2] Six (6) samples were taken from each layer to determine an average GWC value before compaction, [3] Three (3) random samples were taken immediately after compaction of 2-3 lifts

Figure 6 shows the data from EC-5 sensors during the testing period which indicate that the GWC within the embankment had been stabilized before the loading phase of the tests started.
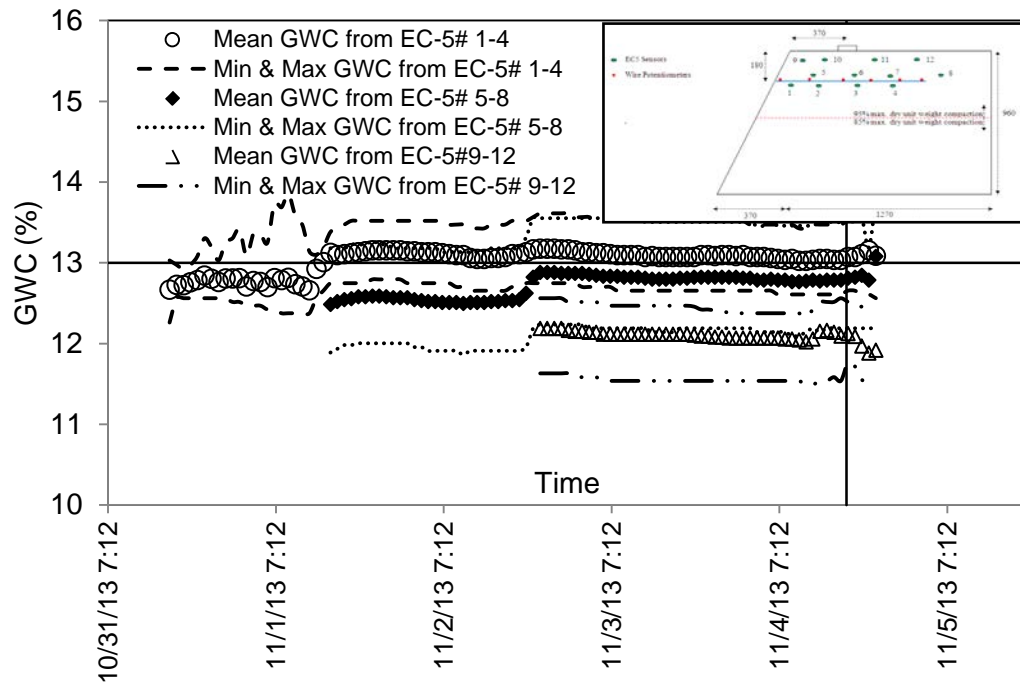
(a)
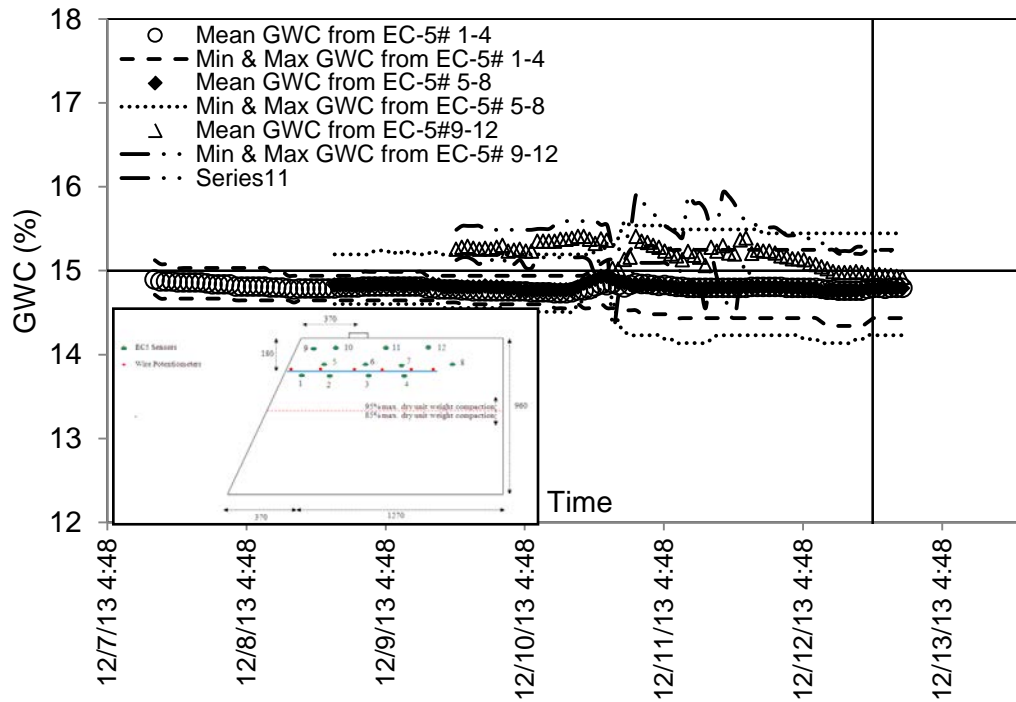
(b)
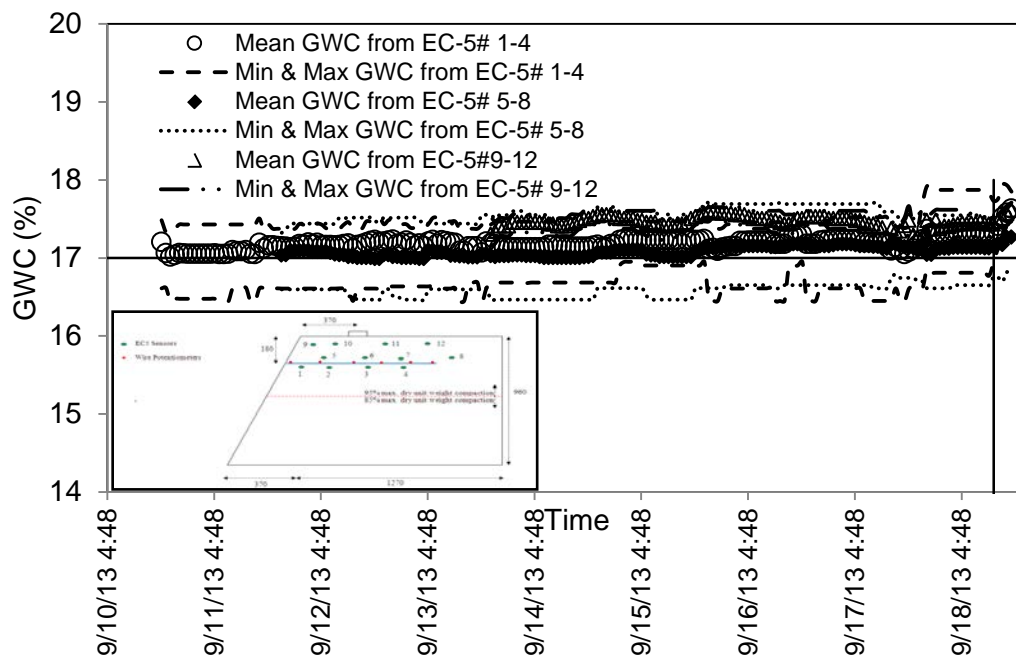
(c)

Figure 6. Average GWC data from EC-5 sensors; (a) OMC-2%, (b) OMC, (c) OMC+2%. Note: The vertical and horizontal lines indicate the time when the loading started and target GWC, respectively.

18

The results in Figure 6 show that the soil water content in the model embankments remained essentially constant for nearly all cases during construction and after loading.

5.1.6.2. LOAD-SETTLEMENT DATA

Figure 7 shows the load-settlement data for all three indoor embankment tests involving the HP570 geotexile reinforcement as compared to the data from earlier similar tests using HP370 (Hatami et al. 2013). The measured compression load is plotted as a function of the strip footing settlement. Failure loads of the embankment models at OMC and OMC+2% for the HP370 geotextile and the OMC-2%, OMC and OMC+2% test cases with the HP570 geotextile were determined using a so-called, tangent intersection method (e.g. Phoon and Kulhawy 2008); an example of which is shown in Figure 7 for the test case at OMC+2% with HP370 geotextile reinforcement (Table 3). Results in Figure 7 and Table 3 show consistently higher footing bearing capacity for the embankment at OMC-2% as compared to the values in the OMC and OMC+2% cases. As expected, higher suction led to a higher bearing capacity in otherwise identical embankment models. Specifically, the bearing capacity values of embankments reinforced with HP370 and HP570 woven geotextiles at OMC+2% were 40% and 33% lower than those of otherwise identical models at OMC-2%, respectively.
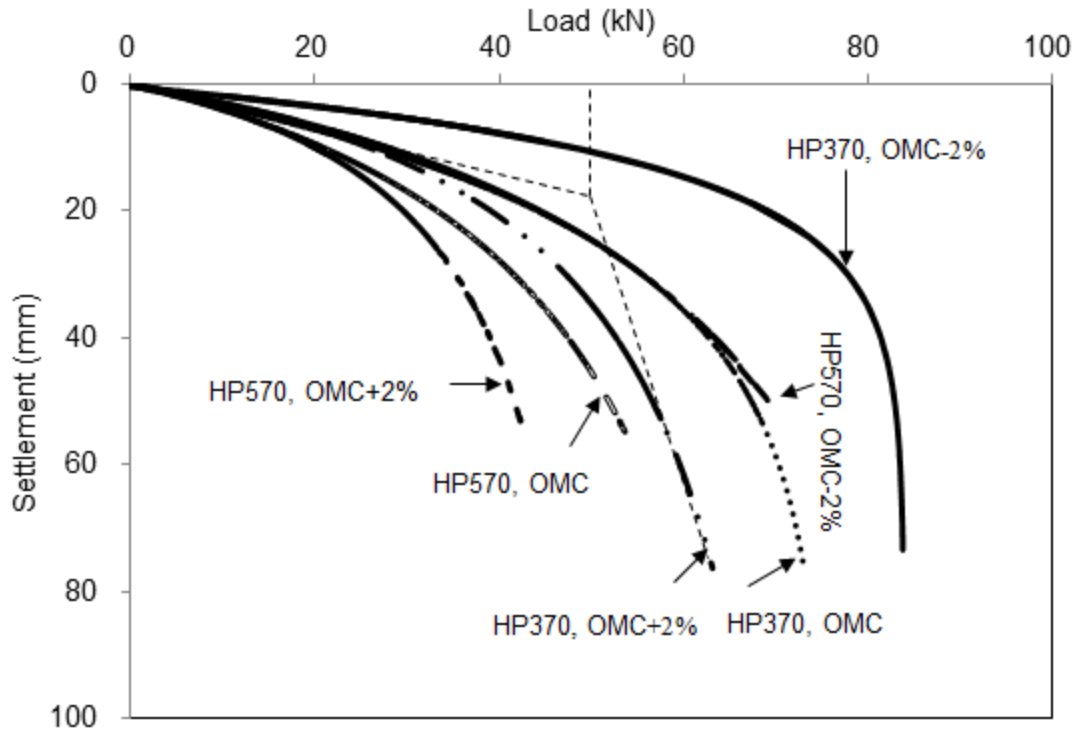
Figure 7. Load-settlement data for indoor embankments at different GWC values.

Table 3. Failure (or maximum measured) loads for embankment models constructed at different GWC values

GWC	Embankment constructed with HP370 (Hatami et al. 2013)			Embankment constructed with HP570		
	Max. footing load (kN)	Failure load (kN)	Settlement (mm)	Max. footing load (kN)	Failure load (kN)	Settlement (mm)
13%	83.6	83.6	45	69.9	51.0	18
15%	73.0	59.0	20	53.8	41.5	20
17%	63.1	49.5	18	42.1	34.0	17

The readings from the EPC sensors are shown in Figure 8. The Boussinesq method (e.g. Budhu 2000) was used to compare theoretical predictions of the vertical and horizontal incremental stresses within the embankment due to a line loading (as given in Equations 5 and 6) with the measured values. With X, Y and Z representing the directions along the running length, width and depth of the model embankments, respectively, the incremental vertical stress in the soil is given by:

$$\Delta\sigma_z = \frac{2qz^3}{\pi(x^2+z^2)^2} \tag{5}$$

Where:

$\Delta\sigma_z$: Increase in vertical stress

q: Vertical line load

z: Vertical distance between the point the stress should be calculated and center of the line load

x: Horizontal distance between the point the stress should be calculated and center of the line load

$$\Delta\sigma_y = \frac{2q\vartheta z}{\pi(x^2+z^2)} \tag{6}$$

Where:

$\Delta\sigma_y$: Increase in horizontal stress

ϑ: Soil Poisson's ratio

(a)

(b)

22

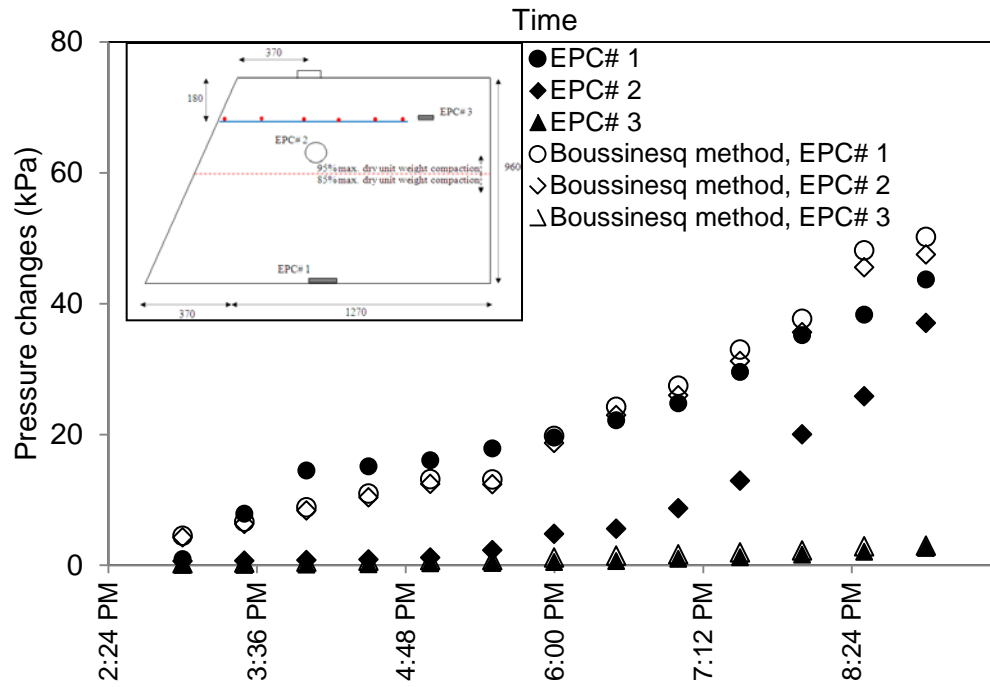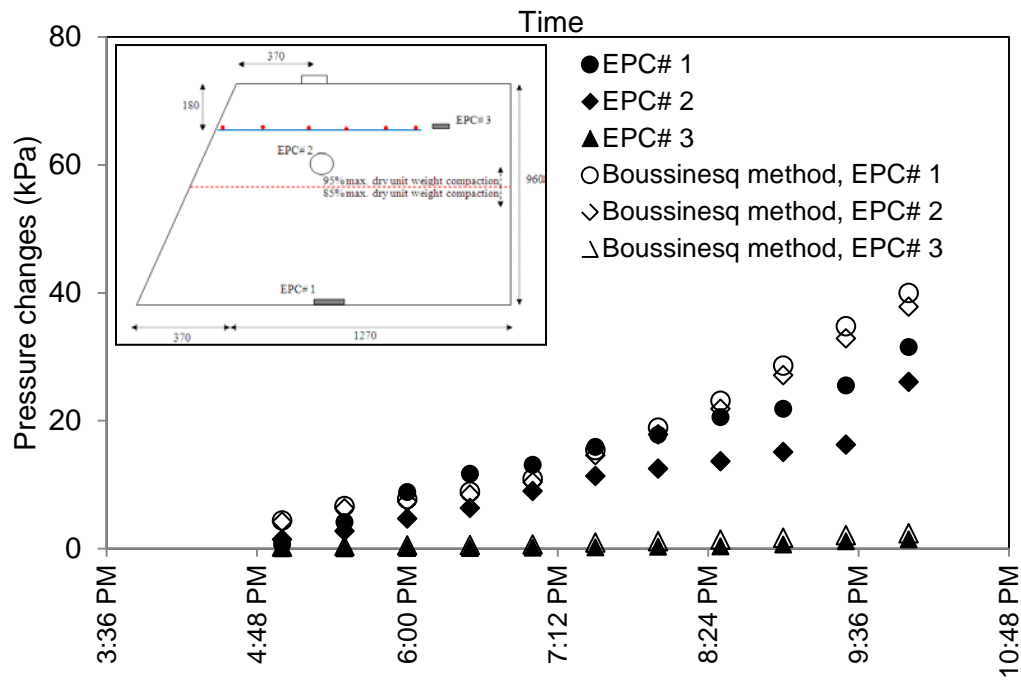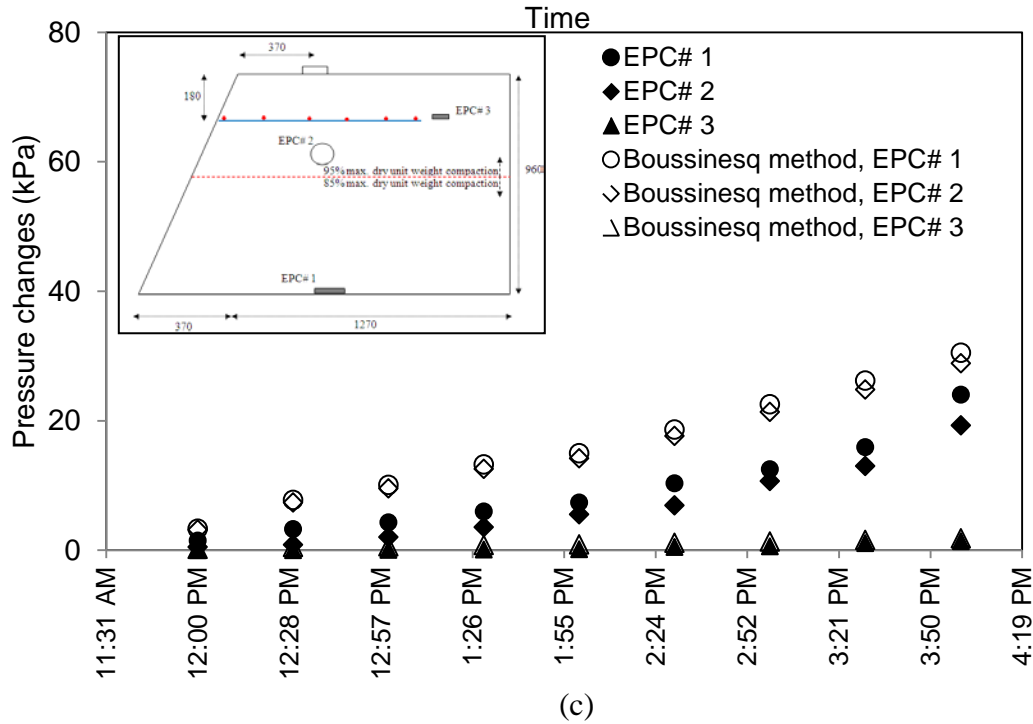Figure 8. Comparison of the measured and theoretical predicted (Boussinesq method) incremental stresses due to the strip footing loading at selected locations in model embankments reinforced with HP570: (a) Test at OMC-2% performed on 01/04/2013, (b) Test at OMC performed on 12/12/2013 and (c) Test at OMC+2% performed on 09/18/2013

Results shown in Figure 8 indicate that the vertical pressures predicted from the Boussinesq equation are greater than the measured values in almost all test cases shown, which could be attributed to the differences between the test setup and Boussinesq's assumptions. For instance, the Boussinesq method is strictly applicable to a line load of infinite length on a semi-infinite elastic and isotropic foundation, whereas in the embankment tests of this study, the line load is finite in length and it is applied near a sloped boundary.

5.1.6.3. STRAIN DISTRIBUTIONS

Geotextile strains and local displacements were measured using six (6) wire-line extensometers attached to different locations along the reinforcement length (Figure 9). The failure wedge in all embankment models tested involved a bilinear slip plane that originated from the upstream side of the footing beam on the top of the embankment and was intercepted by the reinforcement

layer, forming a two-part wedge sliding block bracketed by the slip plane and the embankment facing (Figure 10).
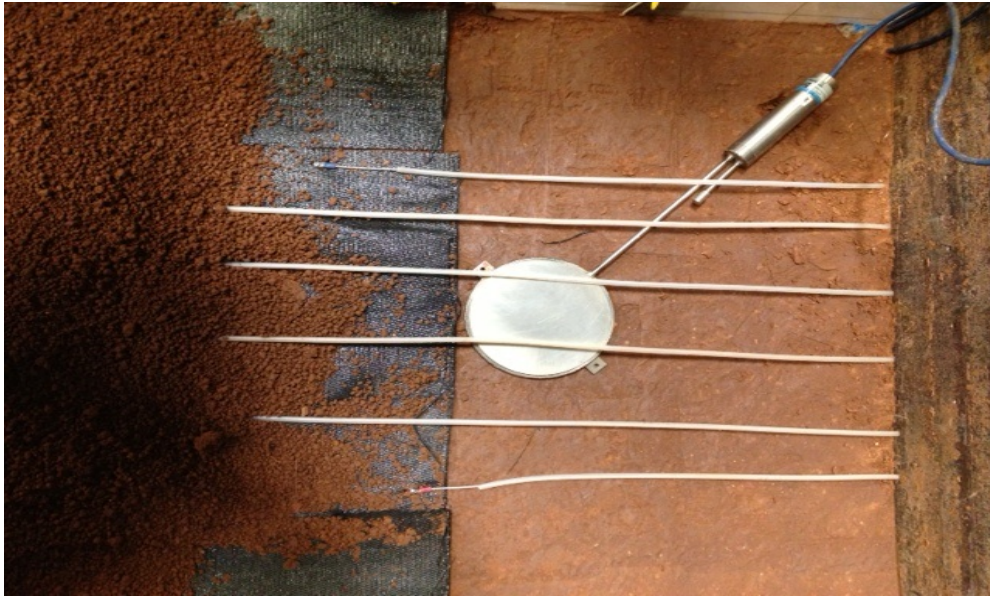
Figure 9. Wire-line extensometers attached to geotextile reinforcement to measure geotextile strains

Figure 10 shows a comparison of failure wedges detected at the end of the surcharge loading stage for the final six indoor embankment tests in the authors' current and recent studies (Hatami et al. 2013 and 2014). Each failure wedge shown is the mean value of geometries that were traced near the sidewalls of the test box and at the center of the model embankment (i.e. mean value of three curves along the running length of the embankment).

After the loading was completed, the loading assembly was removed and the failure wedge was carefully excavated. The transparent Plexiglas sidewalls helped to trace the failure wedges prior to excavation so that any additional cracks as a result of the excavation process could be eliminated from the analysis. In all test cases, the failure wedges initiated at the back (i.e. upstream) of the loading beam and propagated downward until they were intercepted by the geotextile reinforcement. The bottom side of the resulting two-part failure wedge sheared horizontally along the soil-geotextile interface as opposed to penetrating through the geotextile. Since negligible movement was detected by the extensometer outside of the failure wedge (i.e. WP #6), the observed failures were considered primarily as a combination of shear failure within the soil along the dipping segment of the slip plane and along the soil-geotextile interface. It is

24

worth nothing that the occurrence of sliding shear along the soil-reinforcement interface as a consistent failure mechanism in all reduced-scale indoor embankment tests indicated a successful design of the test setup (including factors such as the footing setback and location of the single reinforcement layer within the embankment) with the objective to study direct shear behavior of the unsaturated soil-reinforcement interface in an actual embankment setting that could be compared with the corresponding DST results from the authors' earlier studies (see Section 6.1.3).
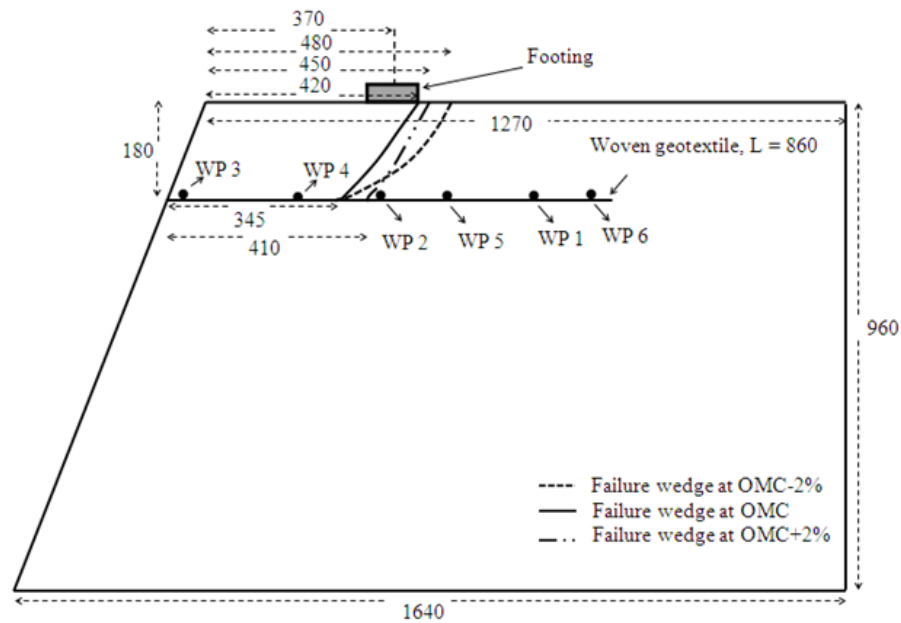
(a)
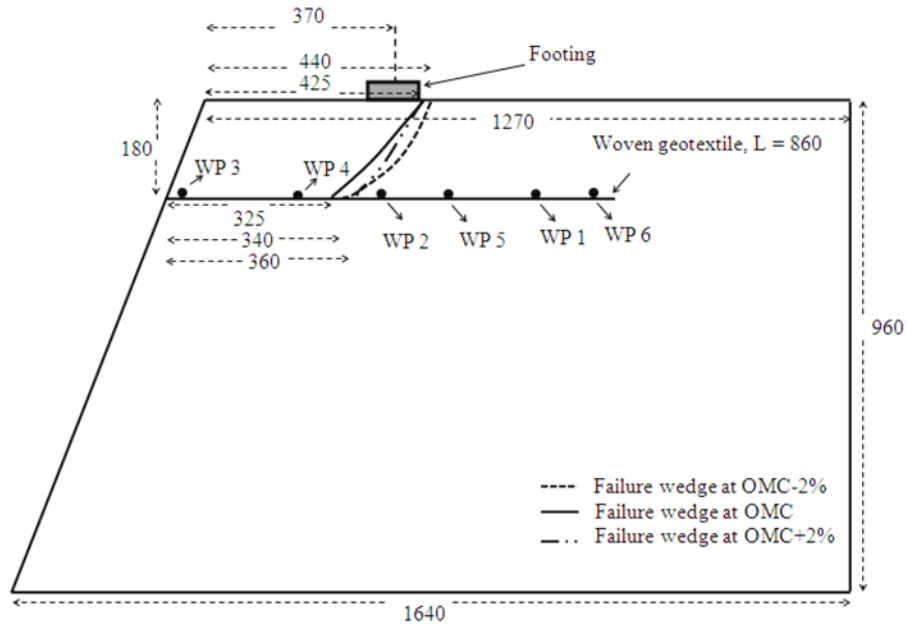
(b)

Figure 10. Failure planes observed in the indoor model embankments: Comparison of failure plane geometries as traced after excavation of failed block at the end of each test for model embankments with (a) HP370 and (b) HP570 geotextile reinforcement

Figure 11 shows strain distributions over the length of the geotextile reinforcement corresponding to the maximum strip footing load. Results in Figure 11 indicate that reinforcement strains in both series of tests (i.e. those with HP370 and with HP570) are greater at higher matric suctions and lower gravimetric water contents due to greater interface strength properties in drier soils.
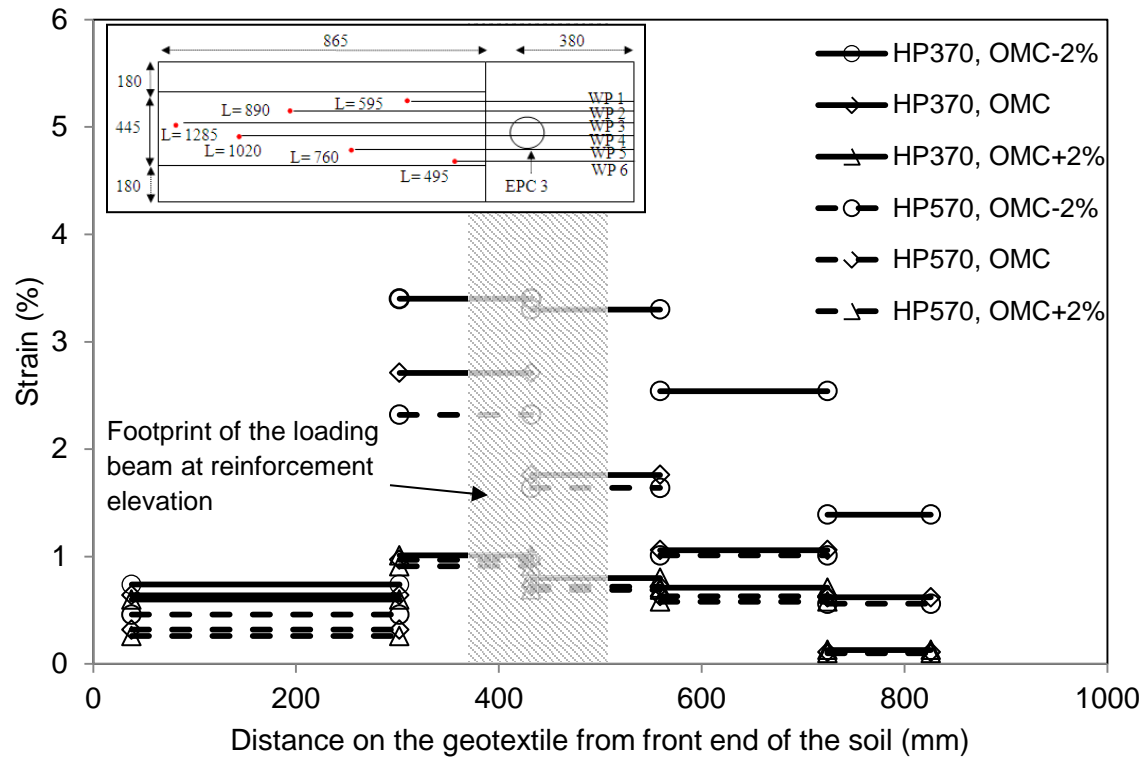
Figure 11. Strain distributions in the geotextile reinforcement in different model embankments

5.2.   LARGE-SCALE OUTDOOR EMBANKMENT TESTS

5.2.1. TEST EQUIPMENT

Different design alternatives were initially explored for the large-scale test unit including a steel test box, an embankment pit and finally, a reinforced concrete test box which was selected as the final design alternative. This selection was made considering the project needs (e.g. a practically rigid test box) and value as a long-term investment for future projects. The reinforced concrete design alternative of the outdoor testing unit was finalized for this study and its structural design was carried out by Dr. Christopher Ramseyer, P.E. (Director of the Fears Laboratory). The nominal dimensions of the test box (Figure 12) are 5 m (L) × 3 m (W) × 2.8 m (H). The walls on all sides of the test box are 0.3-m thick with the exception of two 0.45-m thick wing walls on the sides on which base plates for the loading frame are mounted. The loading assembly is comprised of a steel loading frame together with two 180-ton hydraulic cylinders that were purchased from Enerpac Company (Figure 12a). The cylinders are attached to a 1.7-hp semi-automatic electric pump and ancillary controls. A 32-channel data acquisition system is housed on the side of the test box as part of the outdoor test station. An access earth ramp was built to facilitate the transportation of processed soil to the test box for the construction of the test embankments (Figure 12b).

(a)

(b)

Figure 12.   Test box and loading frame fabricated for the large-scale reinforced embankment tests; (a) Mounting the loading frame, (b) Ramp for transporting soil to the test box using a front loader

5.2.2. MATERIAL PROPERTIES AND INSTRUMENTATIONS

The experience with Chickasha clay in reduced-scale embankment tests indicated that its mixing, processing and compaction for large-scale outdoor models would be time-consuming and therefore it would not be a practical soil for the significantly larger outdoor tests. Additionally, the Chickasha clay soil becomes stiff at lower water contents (e.g. OMC-2%) resulting in reduced influence of reinforcement on the embankment behavior. Therefore, it was decided to search for a more suitable marginal soil in the Norman-OKC area to study the soil-reinforcement interface performance. After communications with selected ODOT field offices and local contractors, a source of soil was identified from excavations in a recently completed I-35/Main Street Interchange project in Norman, OK. Several samples were brought to the OU Soils laboratory and tested to determine the soil gradation, Atterberg limits, Proctor compaction curve and suction values at different gravimetric water contents (GWC). The Liquid Limit (LL), Plastic Limit (PL) and Plasticity Index (PI) of the soil samples were found to be 18.3, 16.7 and 1.6, respectively. The target range of PI values for a suitable range of matric suction and plastic behavior was identified to be between 4 and 10. Therefore, it was decided to mix a small amount of high-grade sodium bentonite (SUPER GEL-X) with the soil to produce a soil mix with

desired ranges of matric suction and plasticity index. Several portions of SUPER GEL-X were blended with the soil sample and it was eventually determined that a mixture of 98% soil and 2% SUPER GEL-X would produce a desired mix with PI = 7.8 and 500 to 900 kPa of suction for the GWC values within the range between 8.1 and 12.1 (i.e. OMC±2%).

Subsequently, 40 cubic meters of the soil from the I-35/Main St. project and twenty five 22-kg bags of SUPER GEL-X were obtained and transported to the Fears laboratory to prepare and process for large-scale embankment tests (Figure 13).
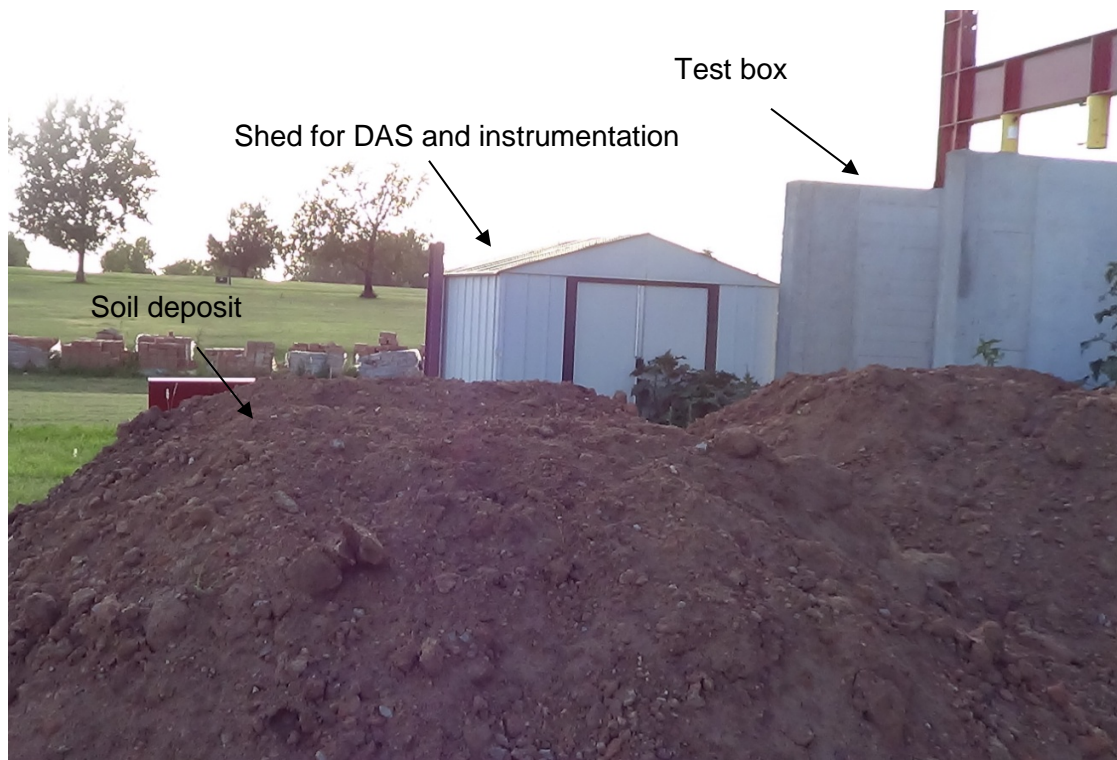
Figure 13. Soil deposit at Fears laboratory for large-scale reinforced embankment tests

A series of sieve analysis, hydrometer tests and modified proctor tests was carried out on the blended soil with 2% SUPER GEL-X with the results as shown in Figure 14. The soil is classified as SC (or A-2-4) and its physical and mechanical properties are summarized in Table 4.
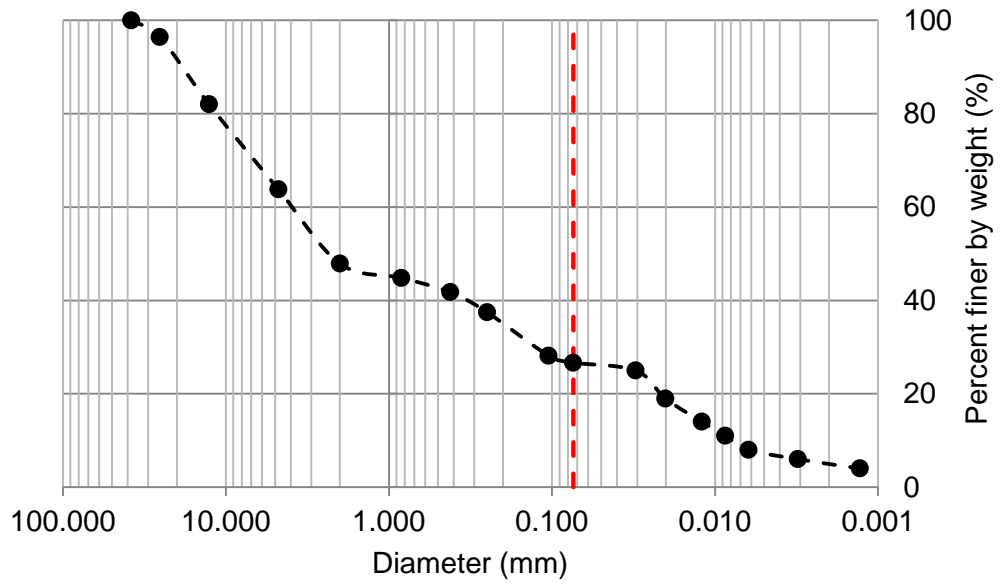
(a)
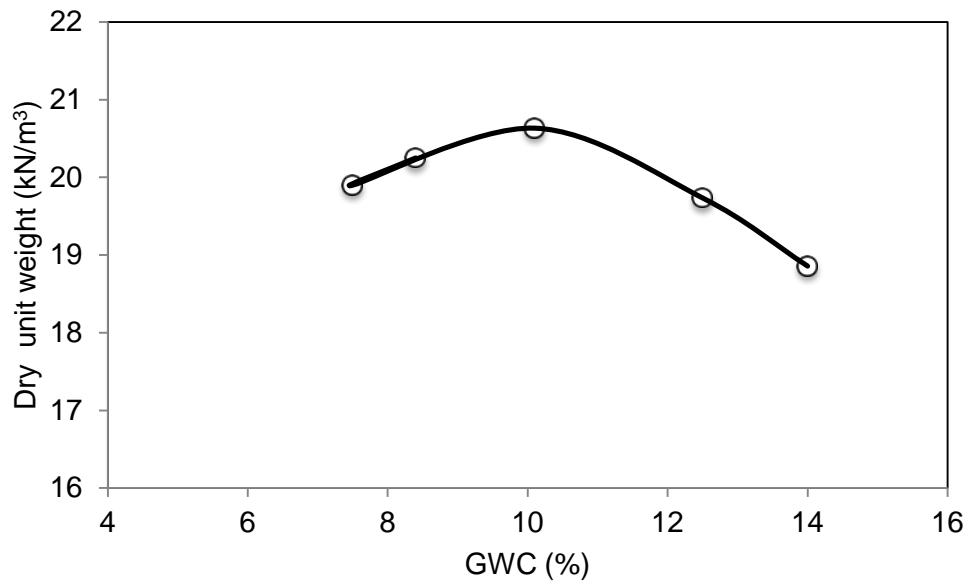
(b)

Figure 14. (a) Gradation curve from sieve analysis and hydrometer tests on sand, (b) Maximum dry unit weight and OMC of sand from modified proctor tests. Note: Dashed line in 'a' indicates Sieve #4 opening size.

Table 4. Selected properties of the soil used for outdoor embankment tests in this study

Property	
Liquid Limit (%)	24.7
Plastic Limit (%)	16.9
Plasticity Index (%)	7.8
Specific Gravity	2.65
Gravel (%)	36.2
Sand (%)	37.1
Silt (%)	21.7
Clay (%)	5
Maximum Dry Unit Weight, kN/m^3	20.6
Optimum Moisture Content (%)	10.1
Cohesion at OMC-2% and OMC+2% (kPa)	12.2, 10.8
Friction angle at OMC-2% and OMC+2% (°)	37.5, 34.3

The outdoor reinforced embankments were constructed using the HP370 geotextile as the reinforcement layers. The same reinforcement material had been used in an earlier series of indoor embankment tests (Hatami et al. 2013). The model embankments were constructed and surcharge loaded at GWC values equal to OMC-2% and OMC+2%.

Three (3) EPC sensors and three (3) LVDTs were used in the full-scale embankments to measure the vertical pressure within the embankment and to monitor the vertical deformation of embankment surface near the loading beam, respectively. Sixteen (16) wire potentiometers (WPT) were attached to four (4) layers of reinforcements to measure their local displacements and strains. Two WPTs also were used to measure the footing settlement (Figure 15).

(a)
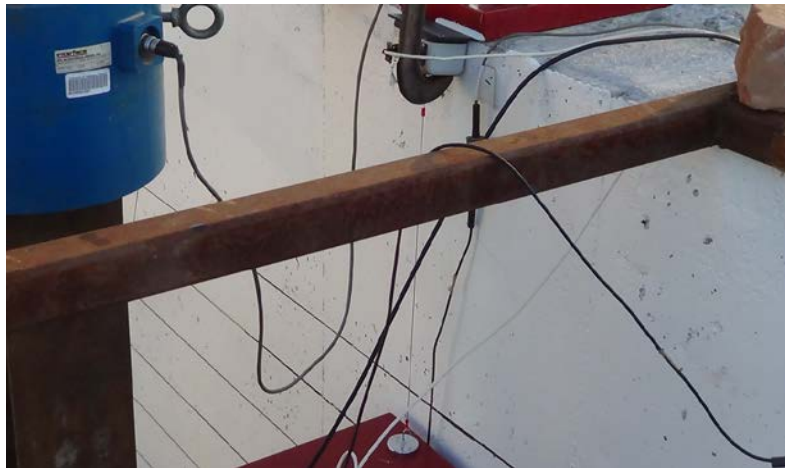
(b)

Figure 15. (a) WPTs installed at the back of the test box to measure geotextile local displacements, (b) WPT used to measure footing settlement

Nine (9) EC-5 sensors were placed near the soil-geotextile interfaces to monitor the GWC during the construction and loading phases of the tests. The lateral deformation of embankments facing was monitored by observation and manual measurements by using

reference square plates in 4 rows over the height of the embankment facing. Figure 16 shows the instrumentation plan for the outdoor tests.

(a)

H = 600 mm   H = 900 mm

H = 1200 mm   H = 1500 mm

(b)
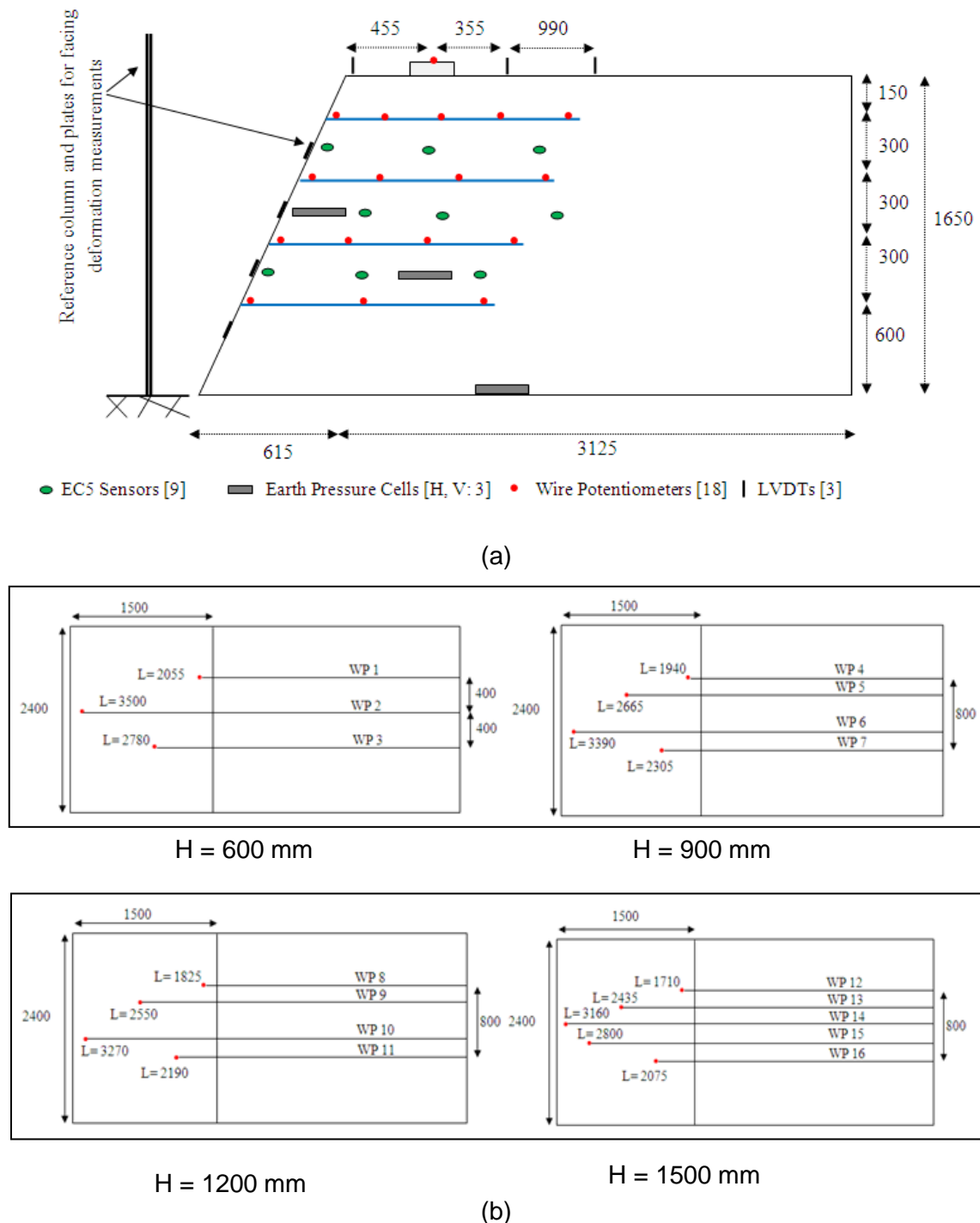
Figure 16.   Instrumentation plan for large-scale reinforced embankment tests: (a) Cross section, (b) Plan view; Notes: [1] All dimensions are in "mm", [2] Length of reinforcement layers throughout the embankment is uniform and equal to 1500 mm, [3] WPs were attached in equal intervals over the length of each reinforcement, [4] Dimensions and locations of sensors are not to scale.

5.2.3. TEST PROCEDURE

The bulk of the soil for the outdoor tests was obtained and transported from the recently completed I-35/Main St. interchange project in Norman, OK to the Fears laboratory at OU. For the construction of each embankment, the amount of soil necessary for two lifts was spread on the ground near the test station and 5 samples were taken from the bottom, top and middle of the soil to determine its initial GWC value. Then, 2% by weight of the SUPER GEL-X sodium bentonite and a calculated amount of water for each target GWC was added and the soil was thoroughly mixed using a rotary tiller. Afterwards, the blended soil was sampled to test its moisture content. Figure 17 shows images from the soil preparation procedure for placement in the test box in the following day.

(a)

(b)

(c)

Figure 17. Preparation of the soil at OMC-2% for large-scale outdoor embankment tests: (a) Sampling for moisture content, (b) Blending the soil with bentonite and water, (c) Covered batch of blended soil for moisture equilibrium before its placement inside the test box

5.2.4. CONSTRUCTION OF EMBANKMENT MODELS

Before constructing the embankment models in the test box, its side walls were coated with polyurethane paint to reduce the friction between the concrete walls and the embankment soil during the tests. The soil was placed and compacted in the test box in eleven (11) 150-mm lifts and to the target value of 95% of its maximum dry unit weight (i.e. γ_d = 20.6 kN/m^3). The

compaction of each layer was carried out in a consistent manner using a Chicago pneumatic rammer (Model 9662) (Figure 18).

(a)

(b)

Figure 18. (a) Placement of the soil in the test box, (b) Compaction of the prepared soil

Each embankment was reinforced with four (4) layers of instrumented geotextile with the uniform spacing of 300 mm. Compaction of each lift took approximately 45 minutes, and oven-drying method, tube sampling and rubber balloon method (ASTM D2167) were used to determine the as-compacted GWC, dry unit weight and degree of compaction of each lift at seven (7) different locations (Figure 19). Figure 19a shows the geogrid template used for a consistent sampling pattern throughout the embankment during its construction. The compacted soil inside the test box was covered with a heavy duty tarp every day before leaving the site to preserve the soil moisture content (Figure 20).
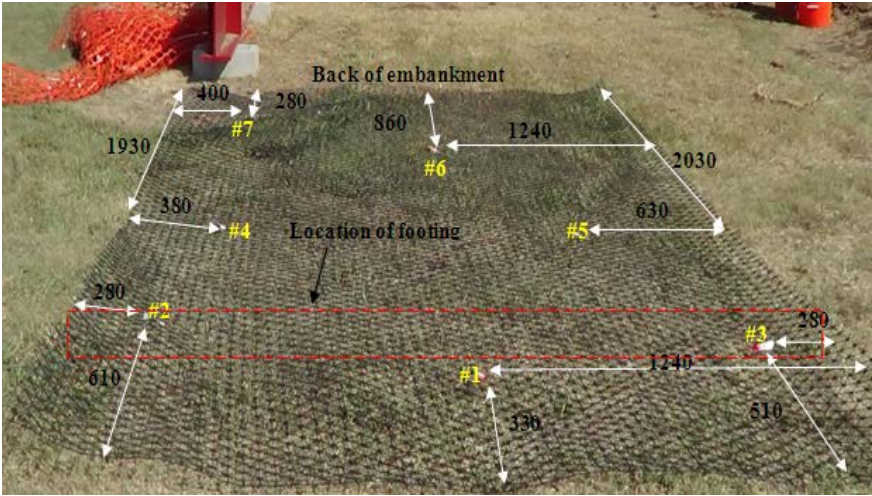
(a)

(b)

(c)

Figure 19.   (a) Locations of moisture and density samples in each compacted lift as marked on a reference grid, (b) Tube sampling for density measurements, (c) Rubber balloon method for density measurements. Note: All dimensions in (a) are in "mm".

Figure 20.   Covered embankment with tarp and plastic sheets during construction to preserve moisture content and expedite moisture equilibrium

After the embankment was fully constructed, the embankment facing was trimmed to the target slope to complete the construction stage before the model was subjected to surcharge loading. Eight (8) 25-mm square plates were mounted on the embankment facing to serve as reference points to monitor its lateral deformation during the loading stage (Figure 21).

(a)
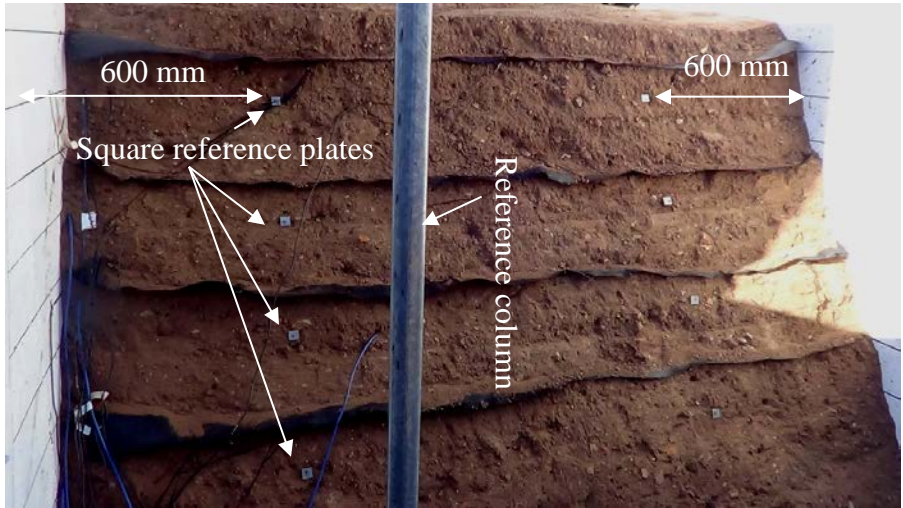
(b)

Figure 21.　(a) Trimming of the embankment facing, (b) Locations of reference plates on the slope

5.2.5. LOADING OF EMBANKMENTS

Before starting the loading phase of the tests, the location of the loading beam on the embankment was leveled and prepared to prevent any uncontrolled rotations of the beam during loading. Afterwards, the beam was moved to the test box using a forklift and it was placed on the embankment 355 mm away from the crest (Figure 22). Two load cells which had been calibrated were placed on the loading beam and were tied to the reaction beam using two long chains to secure them in place after embankment failure. The surcharge load was then applied incrementally on the embankment using two 200-ton, 300-mm stroke hydraulic cylinders (Enerpac Model CLRG-20012) and an Enerpac Electric Pump (Model ZU4420SB; Figure 23). The loading phase continued until a clear and continuous slip surface initiated from the top of the embankment and extended to the embankment facing.

(a)

(b)

(c)

Figure 22. Preparing the loading beam for the test: (a) Leveling off under the beam, (b) Moving the beam to the test box using a forklift, and (c) Location of the loading beam as measured from the embankment crest

Figure 23. The setup of the loading assembly for embankment tests

5.2.6. RESULTS

5.2.6.1. SOIL GWC

GWC value of each soil lift was measured during construction, immediately after compaction and before placing the following lift by taking 7 soil samples from each lift using the oven drying method (ASTM 2216-10). Figure 24 shows the distributions of the soil water content within the large-scale model embankments as measured at designated locations (Figure 19a).
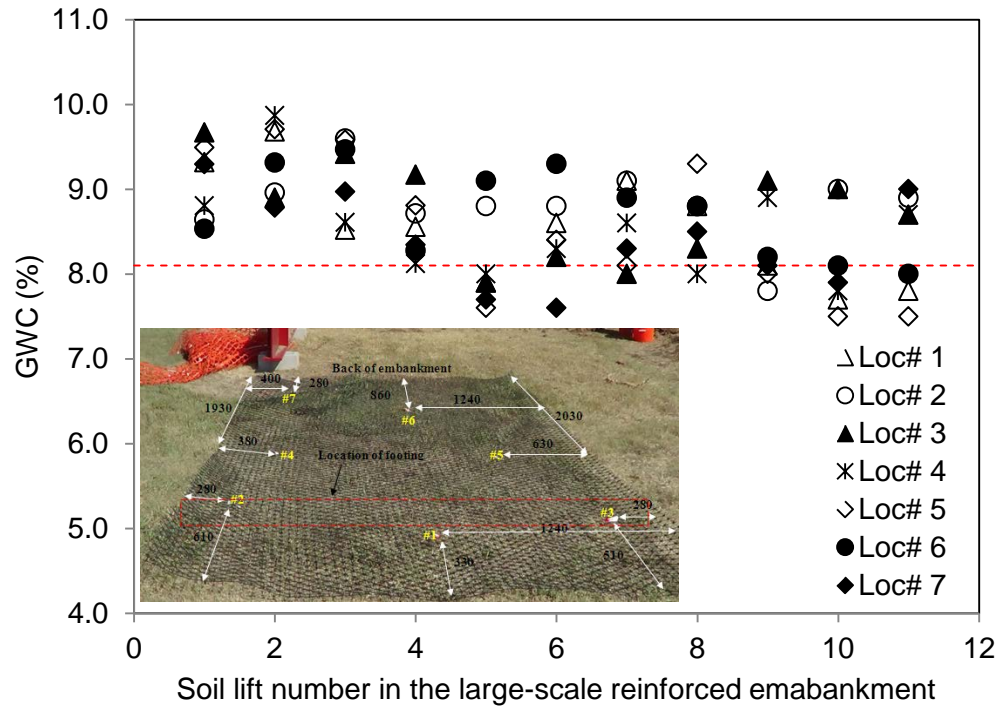
(a)
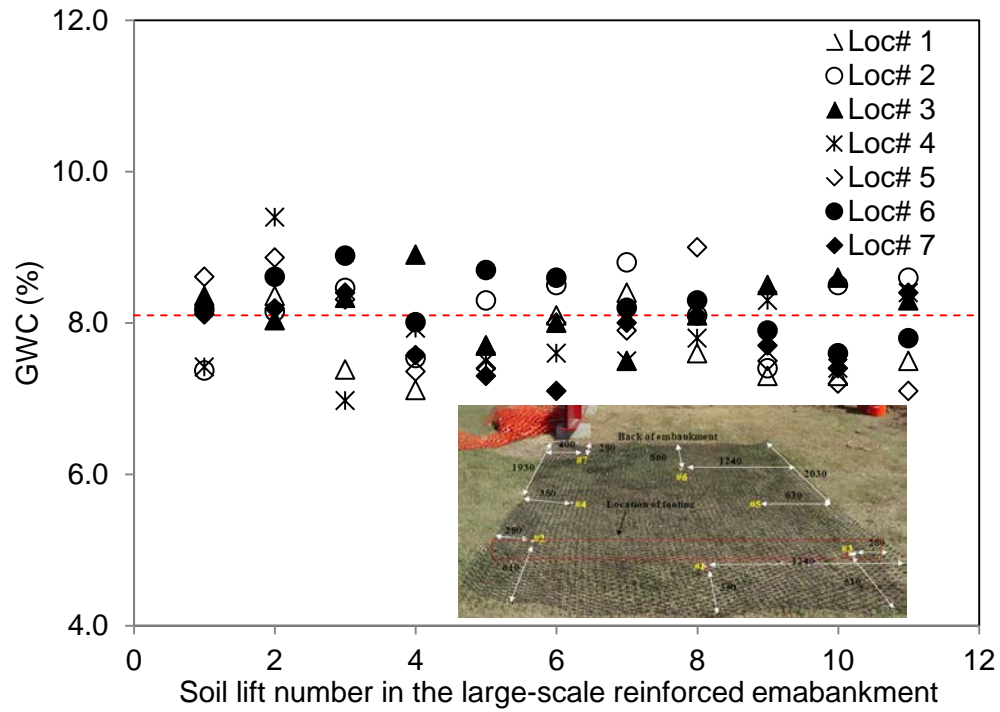
(b)
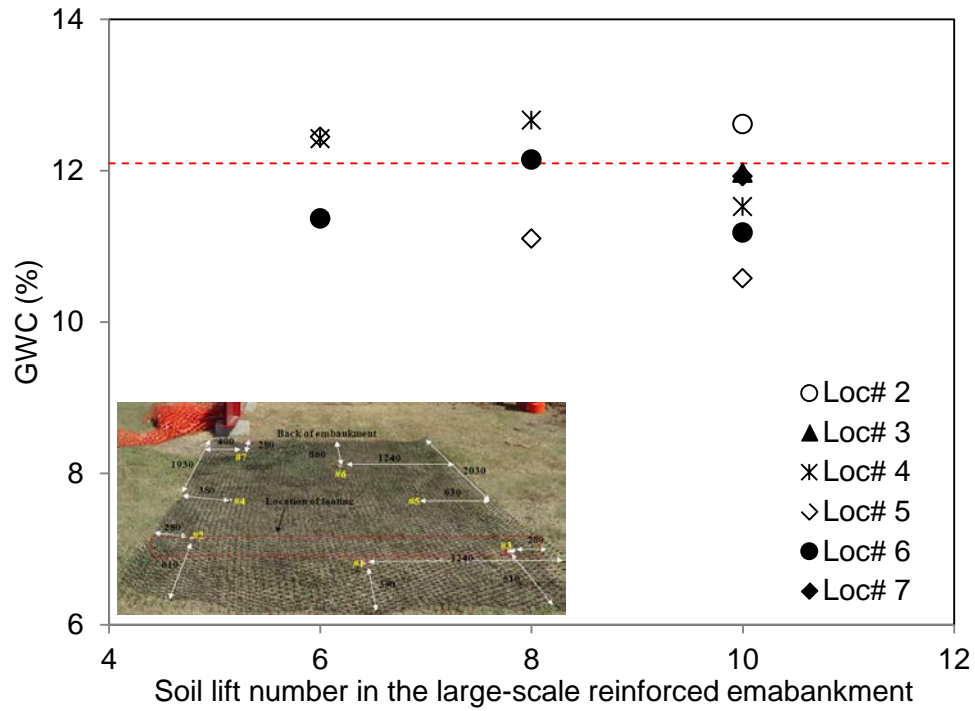
(c)

Figure 24.   Distribution of GWC within the embankment models, (a) Immediately after compaction of each lift, (b) before placement of the next lift (a and b: test case at OMC-2%), (c) After loading and failure of the embankment for the test case at OMC+2%. Note: Horizontal dashed line indicates target GWC value.

Figure 25 shows the data from the nine (9) EC-5 sensors which were used to monitor the soil water content during construction and surcharge loading of the embankment model at OMC-2%. The results indicate that the GWC within the embankment was practically stable and uniform before the loading phase started.
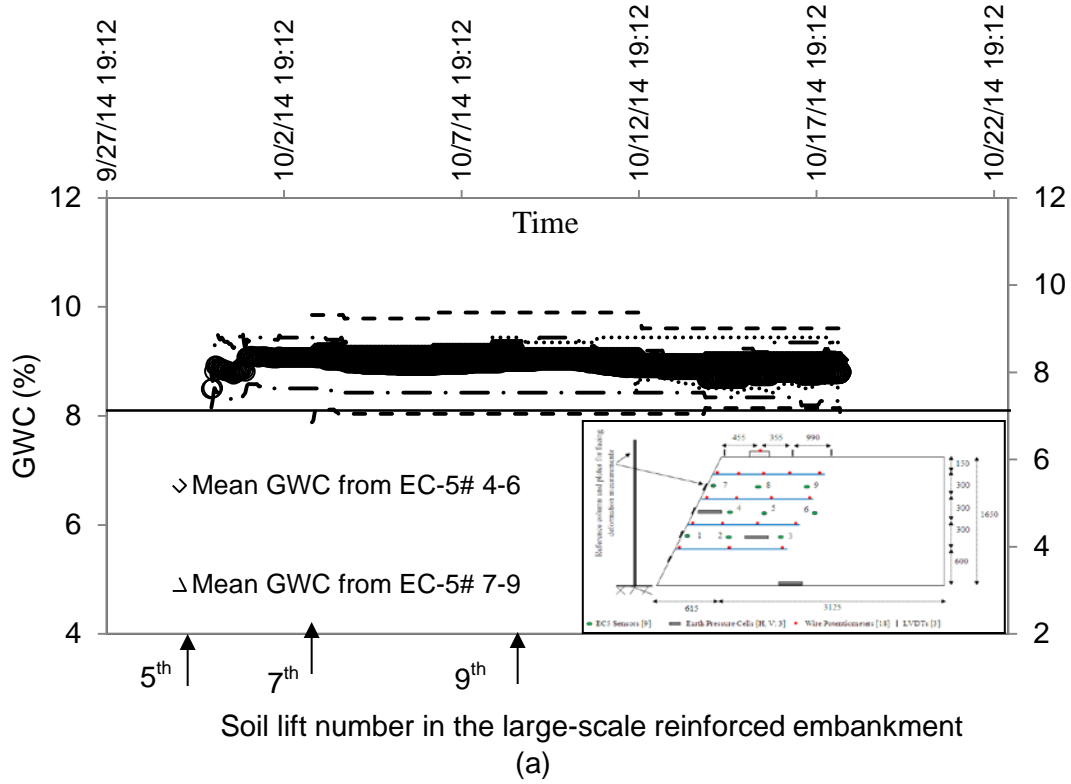
Figure 25. Mean GWC values from EC-5 sensors in the large-scale model embankment constructed at OMC-2%; (a) Construction and loading stages, (b) Loading stage only. Note: The horizontal line in the middle of the graphs indicate target GWC value.

46

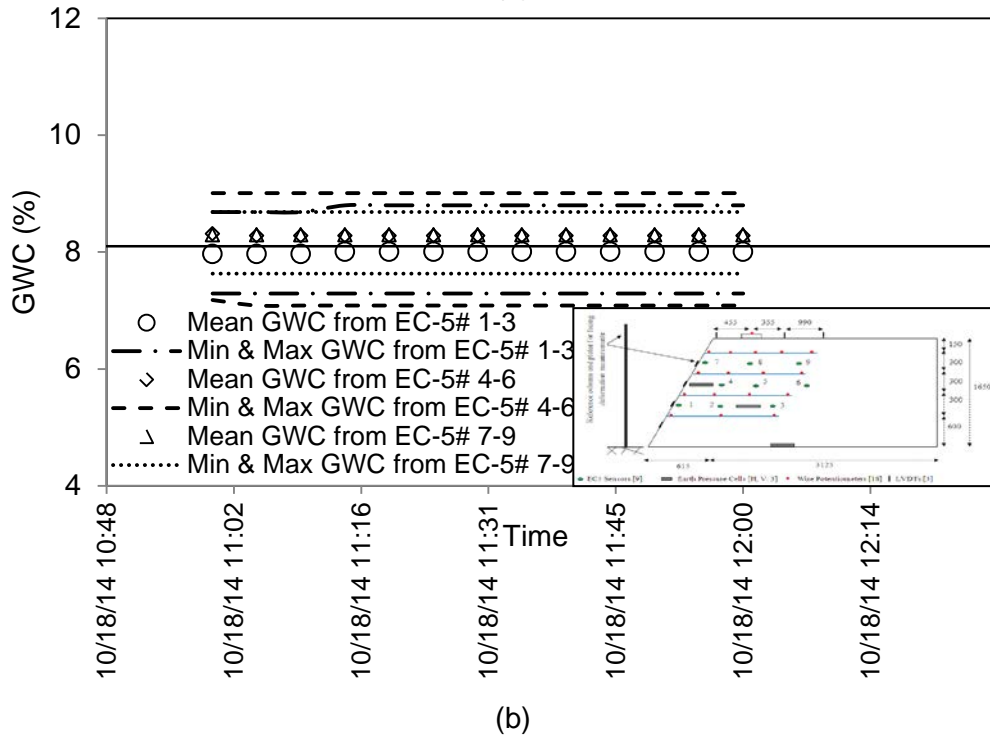Results in Figure 25 show that the GWC value in the model embankment remained essentially constant during construction and after loading.

Figure 26 shows the variations in the soil density and degree of compaction throughout the embankment using brass tube and rubber balloon methods at Locations #1 through #7. Care was taken to compact each lift with consistent effort (i.e. equal passes of compactor equipment). However, measured values for the degree of compaction in Figure 26 indicate that the degree of compaction over the entire embankment varied between 85% and 89% (with equivalent densities between 1750 and 1840 kg/m^3, respectively). Apart from the natural spatial variation of density throughout the embankment, the observed difference could partly be attributed to possible disturbance of the local soil during sampling. Another possible explanation is the difference that invariably exists between the locked-in stresses in the soil near the boundaries of the text box and those in the middle of the embankment plan area.
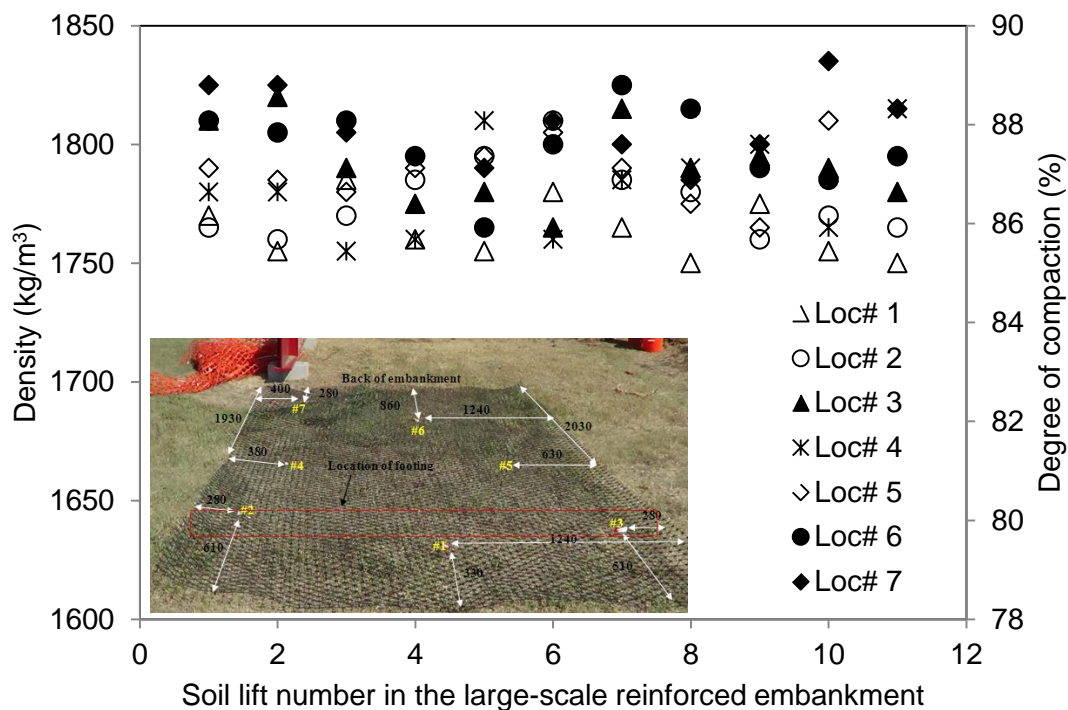
Figure 26. Density results in the model embankment after compaction of each lift

5.2.6.2. LOAD-SETTLEMENT AND EARTH PRESSURE RESULTS

Figure 27 shows the load-settlement data for the model embankments constructed at OMC-2% and OMC+2%. Results indicate that the reinforced embankment tested at OMC+2% showed unexpectedly higher load bearing capacity than the model constructed at OMC-2%. A possible explanation is that the blended soil in the second embankment ended up with a slightly larger concentration of bentonite (i.e. >2%), which indicates that cohesion has a significant contribution in the stability of embankments and reinforced soil slopes. As a result, a series of FLAC/Slope stability analyses was carried out to predict the failure load for the model embankment that was constructed at OMC+2%. Details of those analyses are given in Section 6.2.2.

Figure 27. Load-settlement response of the large-scale reinforced model embankment models

Figure 28 shows the measured (EPC) and predicted (i.e. $\sigma = \gamma z$) earth pressure values within the embankment during the construction and surcharge loading stages. Results in Figure 28a indicate that measured earth pressures at all three locations in the embankment that was tested

at OMC-2% were significantly greater than the corresponding theoretical values. Additionally, the vertical pressures did not in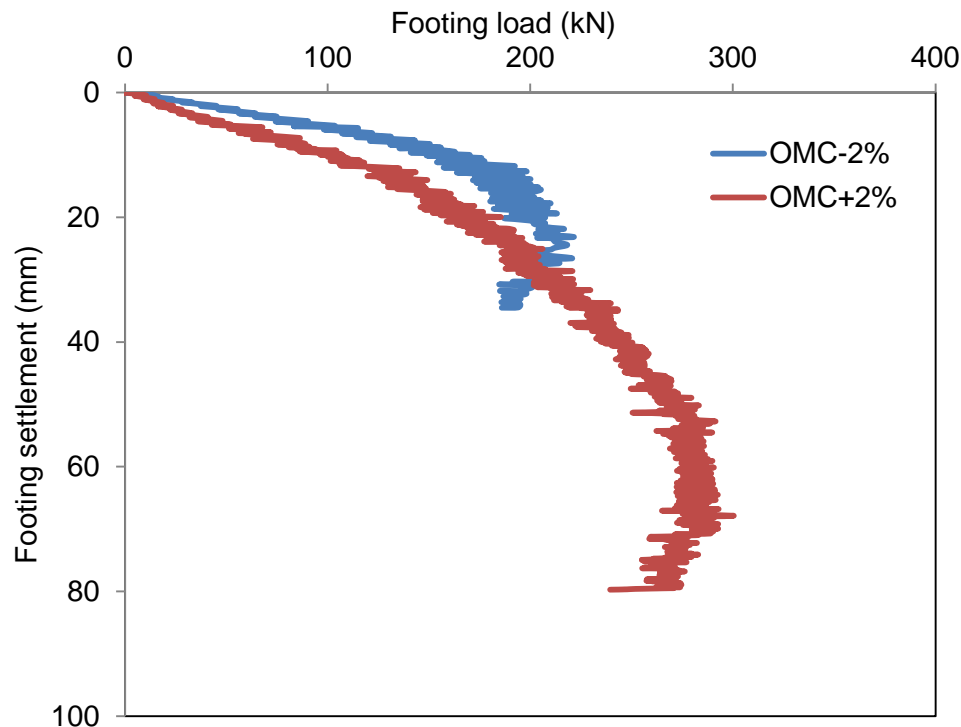crease linearly with the number of lifts that were placed during construction. These observed differences could be attributed to the influences of factors such as the weight and dynamic loading of compaction equipment and construction crew during the construction activity, which resulted in locked-in stresses. It is also observed that the differences between the measured and predicted vertical earth pressures at all locations shown in Figure 28a are more significant earlier on during the construction period and decrease toward the end of construction. This can be attributed to the fact that the influence of construction activity on each EPC diminished as more layers of soil were placed over each sensor during construction. The measured vertical earth pressure at the bottom of the embankment from EPC #1 was 38 kPa which is only 20% greater than the corresponding theoretical value. Results in Figure 28a also show that the maximum difference in vertical earth pressure at the end of construction due to construction activity was recorded by EPC #2 which is approximately 40% of the measured total earth pressure value. Results shown in Figures 26b and 26c indicate that the values of maximum recorded earth pressure at failure at mid-height of the slope (EPC #3) were approximately 35 kPa and 20 kPa for the test cases at OMC-2% and OMC+2%, respectively. These values were approximately 75% and 30% of the values measured by EPC #1 and #2 in the embankment models constructed on dry and wet side of optimum.
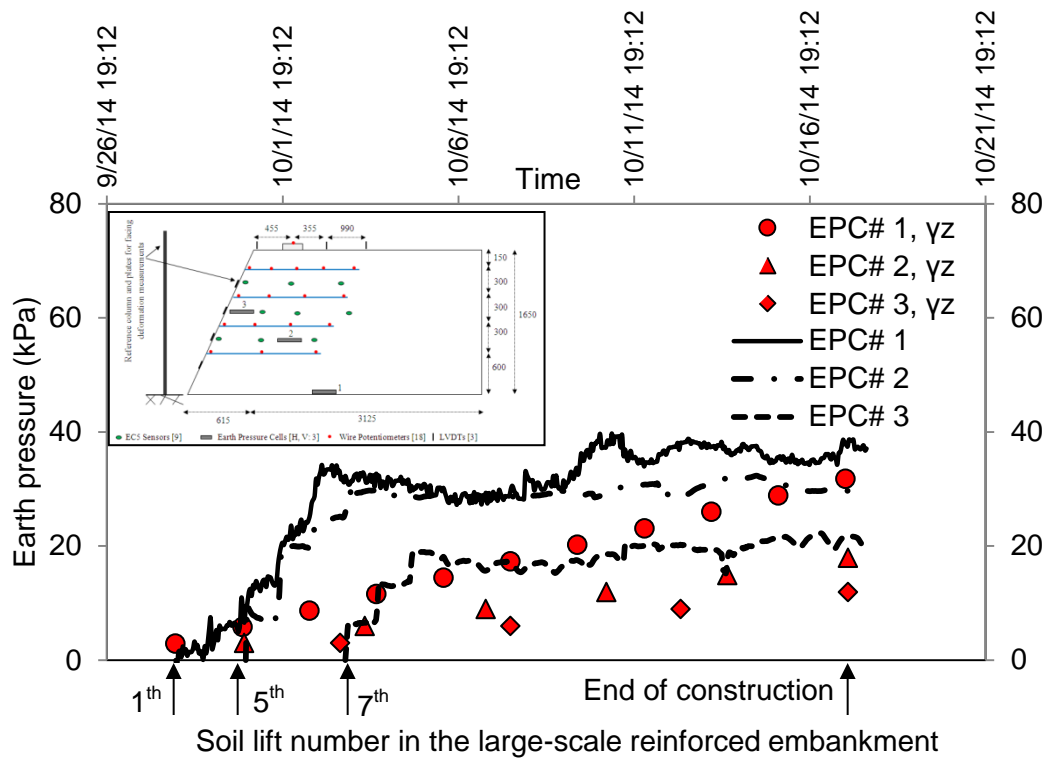
(a)
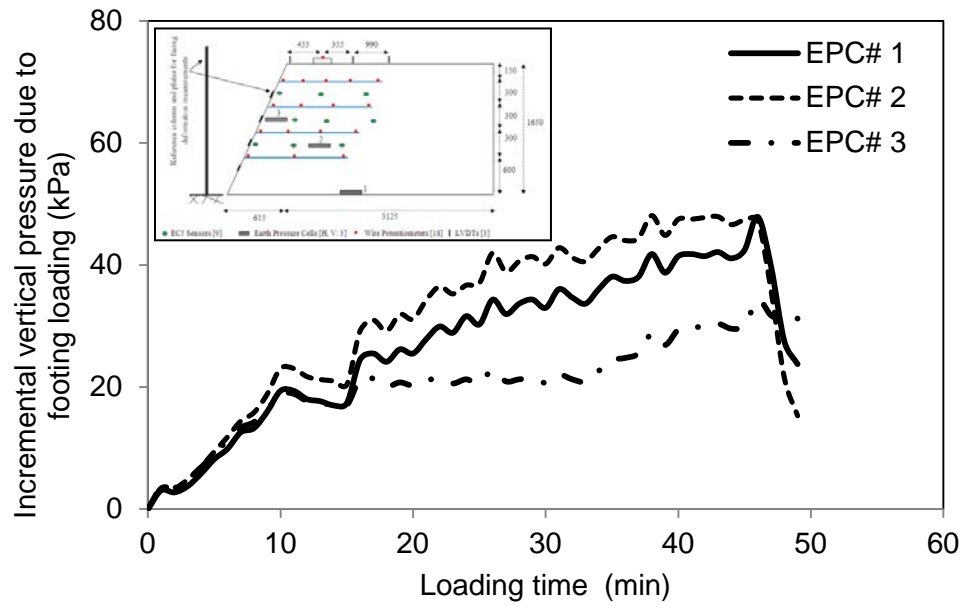
(b)
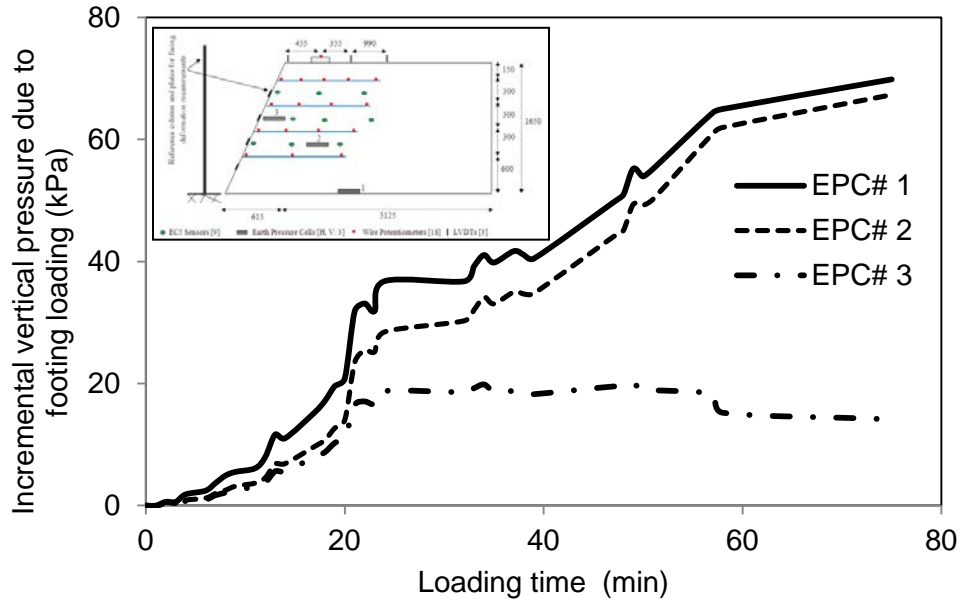
(c)

Figure 28. Earth pressure data in the model reinforced embankments, (a) During construction of model tested at OMC-2%, (b) During surcharge loading of embankment constructed at OMC-2%, and (c) During surcharge loading of embankment constructed at OMC+2%

5.2.6.3. EMBANKMENT DEFORMATIONS

Deformation of embankment near footing was measured using LVDTs at three different locations. Figure 29 shows measured settlements of the embankment top surface during surcharge loading. Results indicate that the embankment surface behind the footing (LVDT 2) settled consistently throughout the loading stage but started to dilate at load levels approaching the failure load. In contrast, LVDT 1 results in Figure 29 indicate that the embankment crest started to heave once the embankment was subjected to the strip footing load. The heaving continued throughout the test but started to reverse into settlement when the embankment approached failure. The LVDT 3 data indicates that the vertical displacement of embankment surface just outside the reinforced mass (1325 mm away from the footing center) was negligible (less than 0.1 mm at failure load). The LVDT results are consistent with the data obtained from reduced-scale embankment models (Hatami et al. 2013).

51
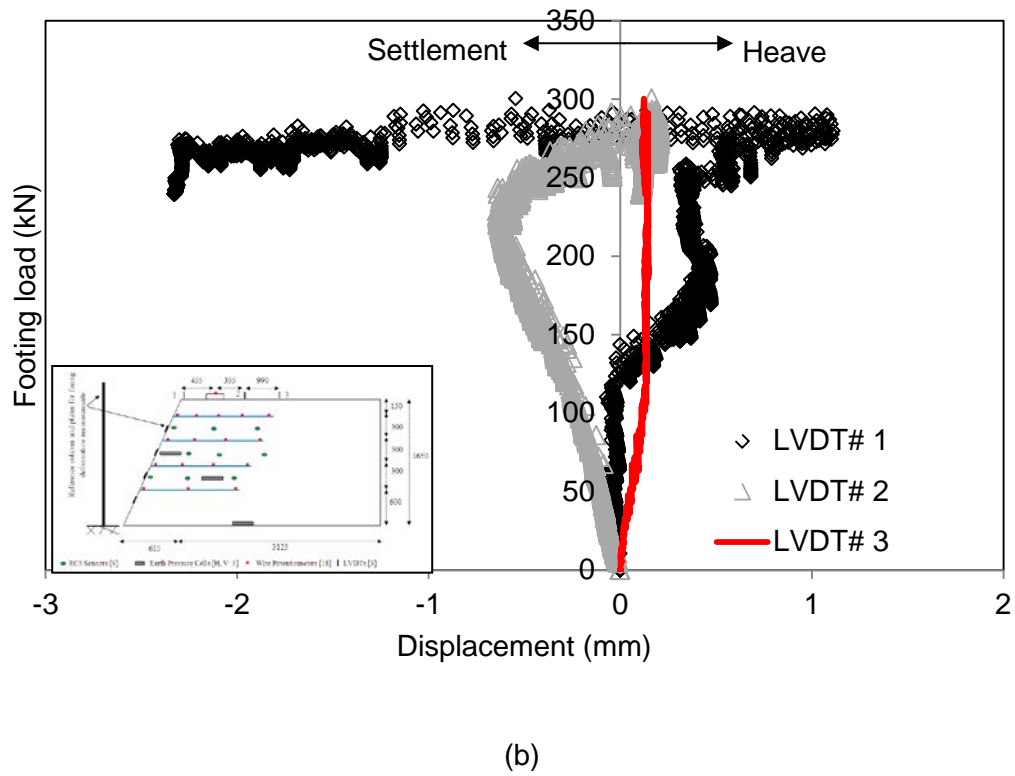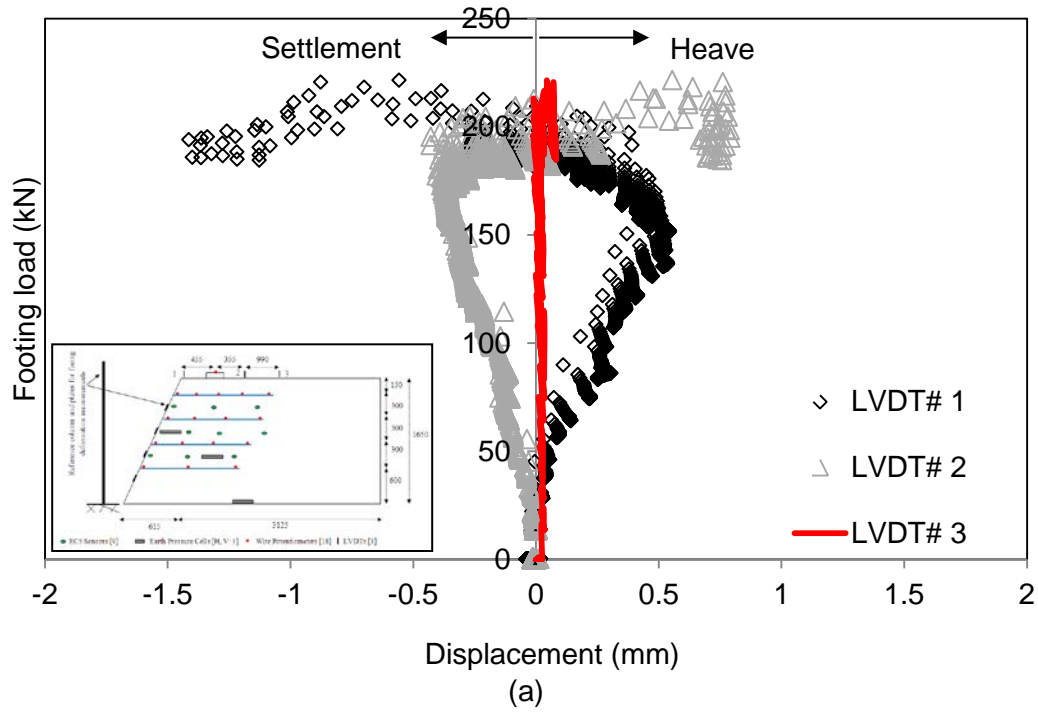
Figure 29. Measured settlements of the embankment top surface near the footing during surcharge loading, (a) OMC-2%, and (b) OMC+2%

Figure 30 shows the facing displacement of embankment model constructed at OMC-2%. Plates #1, 4, 5 and 8 were the bottom left, top left, bottom right and top right reference plates, respectively, as shown in Figure 21b. Two additional plates were mounted at the crest level. However, they fell off the embankment during surcharge loading of test at OMC-2%. Results in Figure 30 indicate that a significant horizontal displacement occurred in the embankment slope 150 mm below the top (i.e. 4th) reinforcement layer. The failed block slid up to between 116 mm and 146 mm outward on the 3rd geotextile layer as measured using 25-mm square reference plates on both (i.e. left and right) sides of the slope facing.
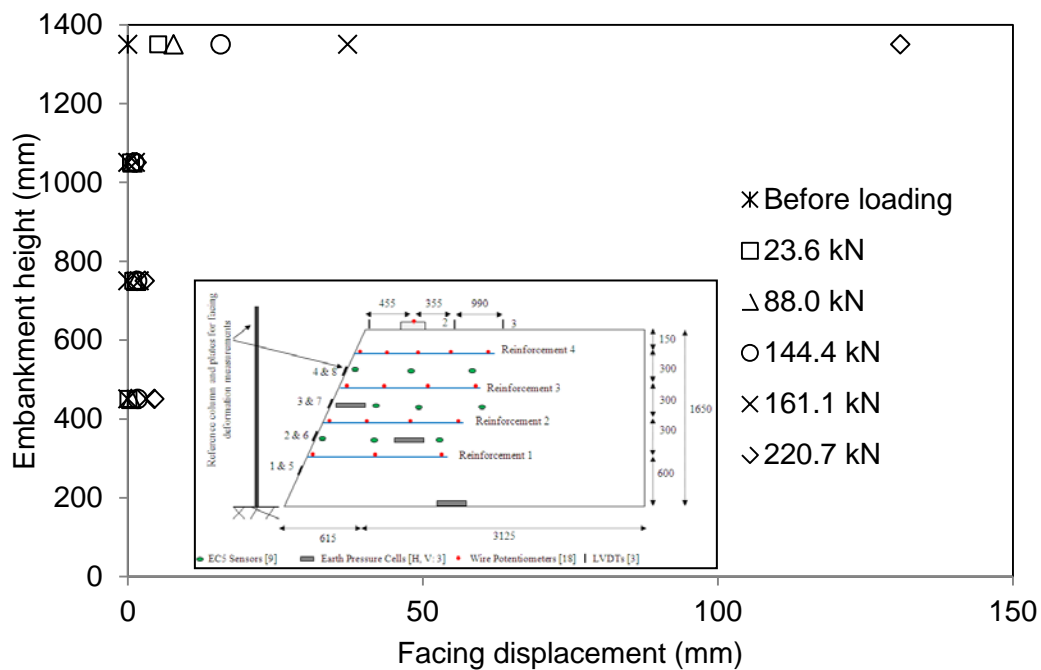
(a)
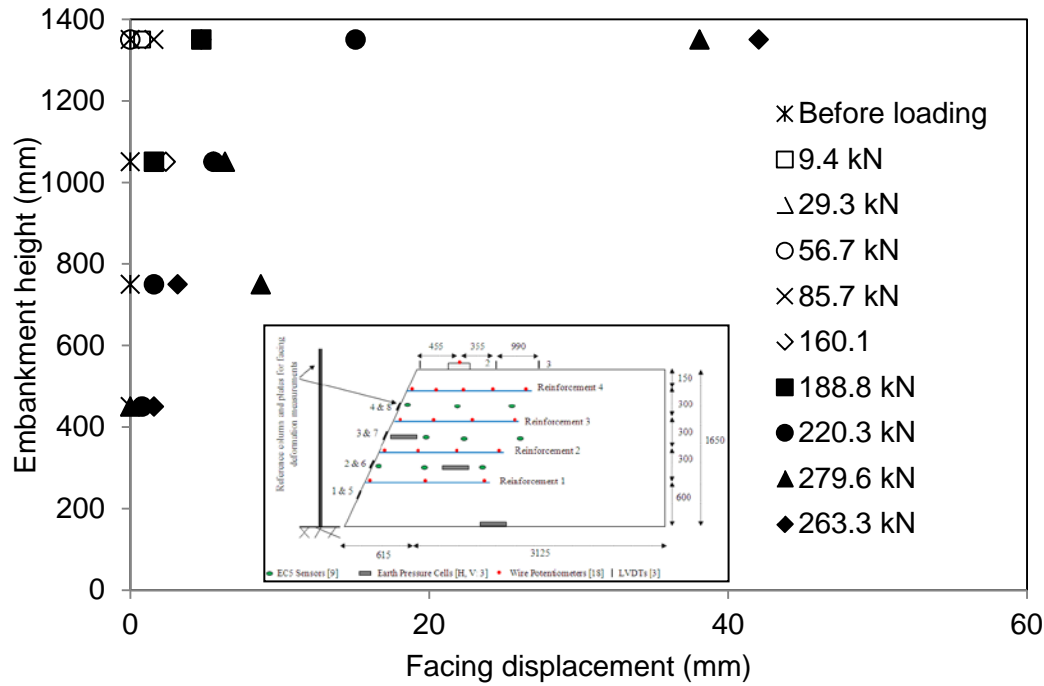
(b)

Figure 30. Facing deformation of embankment model as measured using reference plates; (a) at OMC-2%, and (b) at OMC+2%. Note: The facing displacement on x-axis is determined by taking mean value of left and right reference plate.

5.2.6.4. SLIP SURFACE AND STRAIN IN GEOTEXTILE REINFORCEMENT LAYERS

Figure 31 shows traced geometry of the slip plane during embankment excavation after the end of the surcharge loading test. The failure wedge in the reinforced mass originated from the back of the loading beam on the surface of the embankment and the dipping slip plane was intercepted by the top two (i.e. 3rd and 4th) geotextile layers as shown in Figures 31 and 32. These figures indicate that the failure geometry was complex and involved a combination of soil shearing, pullout interaction and interface shearing along the top geotextile reinforcement, and interface shearing between the soil and the third geotextile layer.
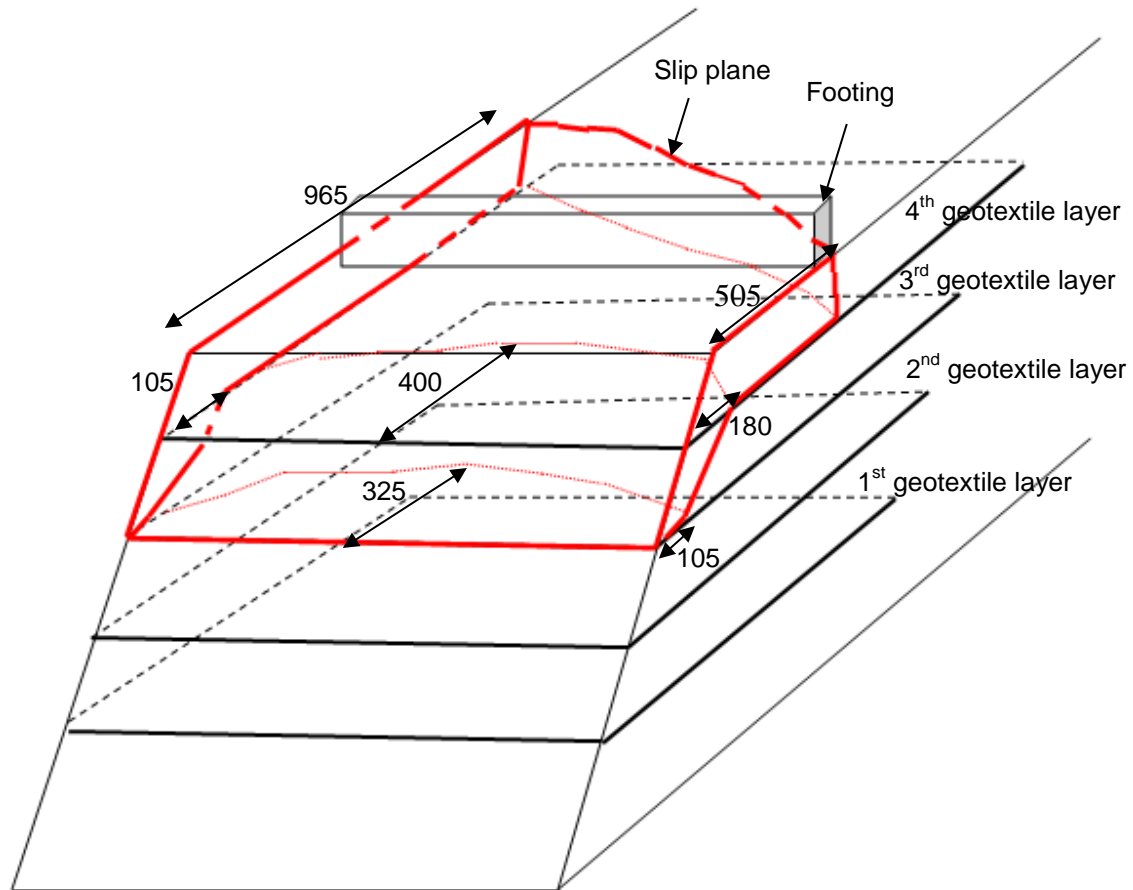
Figure 31. Failure plane geometry as traced after careful excavation of the failed block at the end of the test constructed at OMC-2%. Note: all dimensions are in "mm".

(a)

(b)

4th geotextile layer

Slip plane underneath 4th geotextile
which slid on the 3rd reinforcement
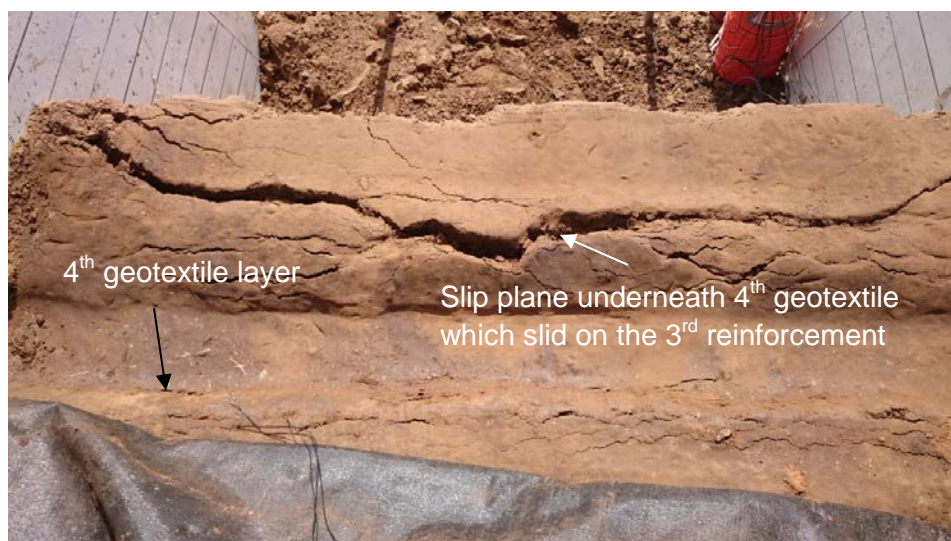
(c)

(d)

Figure 32. Failure wedge in the embankment model tested at OMC-2%; (a) Initiation of slip plane on embankment surface, (b) Excavated part of failure wedge above the fourth layer of geotextile, (c) Continuation of slip plane underneath the fourth geotextile layer and (d) Excavated part of slip plane shown in "c" which slid over the third layer of geotextile

At the end of each test, the loading assembly was removed and excavation was started by carefully removing the soil within the failure wedge (Figure 33).

(a)

(b)

Figure 33. (a) Moving construction equipment out of the test box using a forklift, (b) Digging the soil around sensors during the excavation phase after surcharge loading was completed

Figure 34a shows local displacements of the top (4th) geotextile layer and Figure 34b shows the corresponding strain distributions at failure load over the length of all reinforcement layers for the test at OMC-2%. Results in Figure 34b show that the top geotextile reinforcement experienced a maximum strain of 2.4% at the front end which decreased to 0.4% at its tail end. The strain distributions in the top reinforcement layer which experienced pullout are consistent with those from earlier large-scale pullout tests (Esmaili et al. 2014).
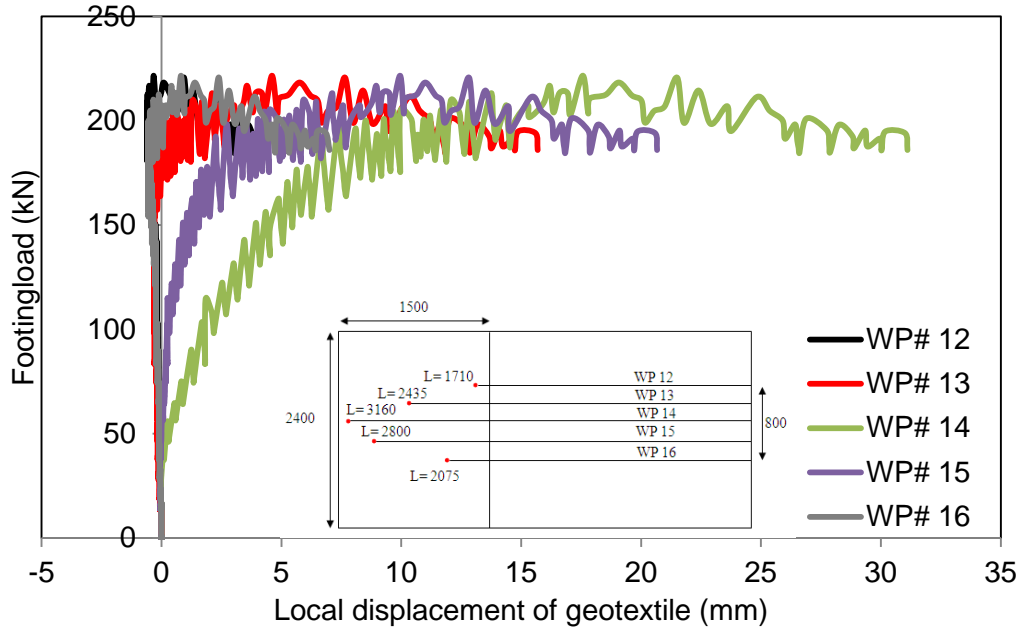
(a)
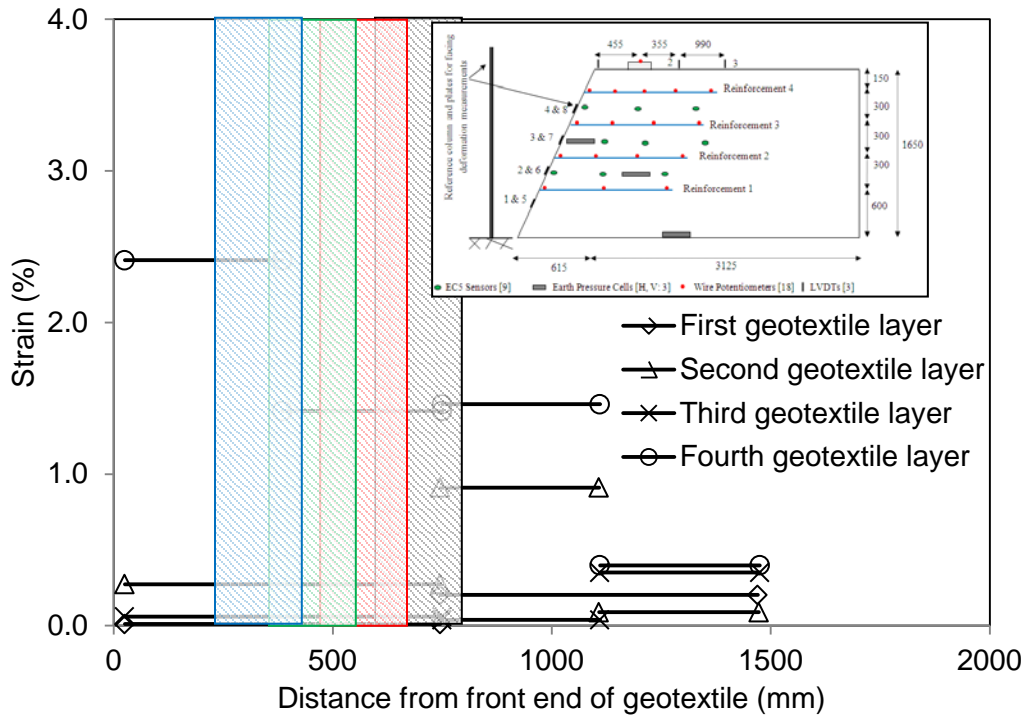
(b)

Figure 34. (a) Local displacement of the top (4th) geotextile layer as measured using five wire potentiometers in the embankment at OMC-2%, and (b) Strains along the length of geotextile layers for model at OMC-2%; Note: Black, red, green and blue indicate the footprint of the loading beam at the 1st (bottom), 2nd, 3rd and the 4th (top) geotextile elevations.

6. SLOPE STABILITY ANALYSIS

6.1. METHODOLOGY

Slope stability analysis was carried out using GSTABL (Gregory Geotechnical Software 2003) to study the stability of large-scale reinforced embankments in the outdoor testing program. The embankments were modeled at two different GWC values of OMC-2% and OMC+2%. The results for the embankment constructed at OMC-2% were validated using the first large-scale outdoor test. The stability of an otherwise identical reinforced embankment constructed at OMC+2% was subsequently predicted using the GSTABL program.

A series of slope stability analyses was carried out with GSTABL using several methods including the Janbu Method of Slices, the General Limit Equilibrium (GLE) and the Bishop method. In contrast to the GLE and Bishop methods which satisfy moment and force equilibriums (the Bishop method does not satisfy horizontal force equilibrium), the Janbu method does not satisfy moment equilibrium and only includes equilibrium of vertical and horizontal inter-slice forces. However, it was found that stability calculations using the Janbu method were more reasonable and comparable to the experimental data in this study.

A series of reduced-scale pullout tests was carried out at different GWC values (i.e. OMC-2% and OMC+2%) and overburden pressures (i.e. 50, 75 and 100 kPa) to determine the pullout capacity of the geotextile reinforcement per unit width (P_r) at different GWC values for GSTABL analysis. Table 5 shows the results of pullout tests on the HP370 geotextile reinforcement in the soil that was used in the large-scale outdoor reinforced embankment tests and the corresponding MRF values.

Table 5. Reduced-scale pullout test data and MRF values for the large-scale reinforced embankment soil and the HP370 geotextile reinforcement at different overburden pressures

	Force in reduced-scale pullout tests P_{r_rs} (kN/m)		
Test Case	Overburden Pressure, σ_v (kPa)		
------------	50	75	100
OMC-2%	0.9	1.4	1.8
MRF	0.77	0.78	0.78

Table 6 shows the input parameters used in the GSTABL stability analysis. The average vertical stress on each reinforcement layer at the laboratory failure load was determined using the Boussinesq method (Budhu 2000) and the P_r values were either interpolated or extrapolated from the pullout test results. The P_r values were determined by prorating the reduced-scale pullout capacity values P_{r_rs} by the ratio L_e/L_p in the form:

$$Pr = Pr\_rs \times Le/Lp \tag{7}$$

where L_e and L_p are the reinforcement embedment lengths in the full-scale reinforced embankment and in the reduced-scale pullout tests (40 mm), respectively.

Table 6. Input parameters used in the GSTABL stability analysis

Soil			Geotextile				
			-------	1st layer	2nd layer	3rd layer	4th layer
OMC-2%	γ (kN/m³)	19.3	P_r (kN/m)	33.8	39.2	46.7	56.4
	c (kPa) φ (°)	12.2, 37.5					
OMC+2%	γ (kN/m³)	20	P_r (kN/m) [1]	26.4	30.5	36.4	44.0
	c (kPa) φ (°)	10.8, 34.3					

[1] P_r values in the embankment at OMC+2% were calculated using the following equation: $P_{r\_OMC+2\%} = P_{r\_OMC-2\%} \times MRF$

6.2.   RESULTS

6.2.1. EMBANKMENT MODEL AT OMC-2%

Figures 35a and 35b show the factor of safety and geometry of failure as obtained from the GSTABL analysis using the Janbu method after applying the observed experimental failure pressure (i.e. 450 kPa). Results in Figure 35b indicate that the analytical slip plane intercepted the top geotextile layer and slid over the third reinforcement, which in this sense is consistent with the observations in the actual large-scale outdoor test. Also, the factor of safety obtained from GSTABL (i.e. FS = 1.086) is reasonably close to unity, indicating impending failure. A possible improvement in both the predicted geometry of failure and the corresponding factor of safety is expected by using a multi-part wedge analysis (as opposed to a circular geometry) which is reserved for a future work.

(a)

63
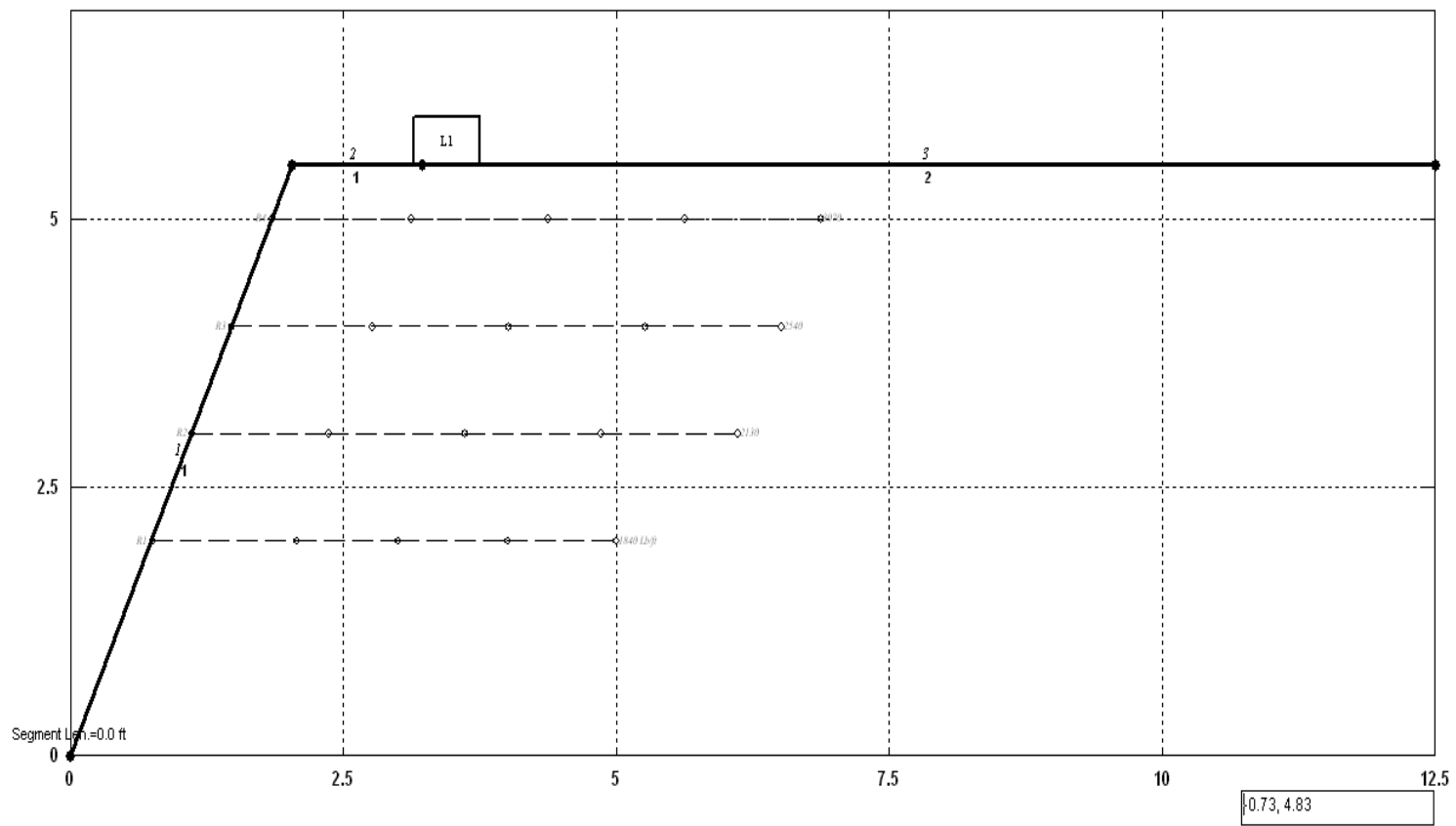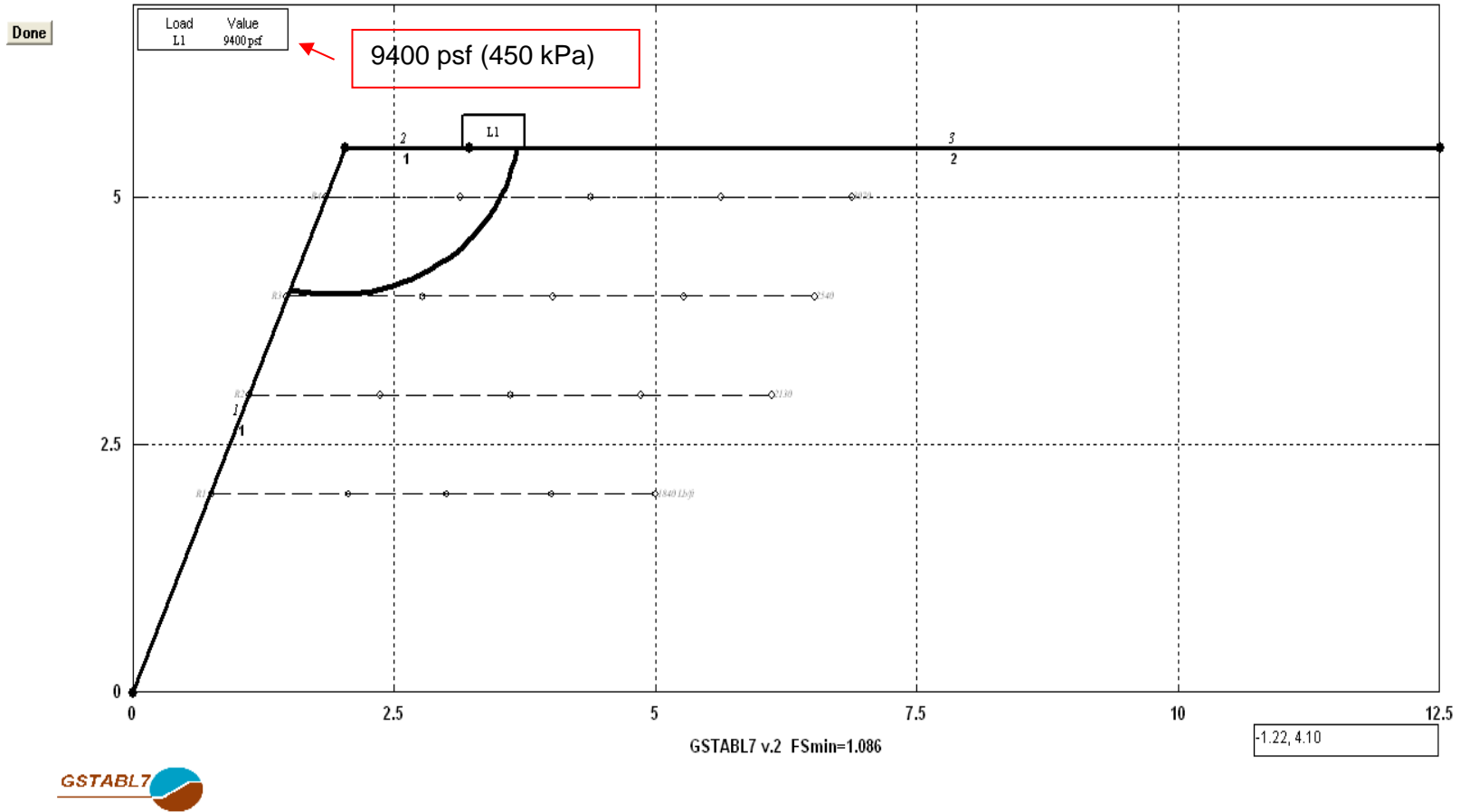
(b)

Figure 35. Slope stability analysis of the outdoor reinforced embankment model constructed at OMC-2% using GSTABL: (a) Model geometry, (b) Critical slip surface and factor of safety

6.2.2. EMBANKMENT MODEL AT OMC+2%

Figure 36 shows predicted slip surface and factor of safety within the embankment as it was subjected to the laboratory failure pressure of 450 kPa. Results in Figure 36 indicate that the MRF value applied to the soil-geotextile interface lowered the factor of safety from 1.086 to 0.937 and show that the embankment constructed on wet side of optimum would be unstable when subject to footing pressure of 450 kPa. Figure 37 shows that the surcharge load needed to reach the same factor of safety obtained for the OMC-2% model (FS= 1.086) for the case of embankment constructed at OMC+2% is 320 kPa. The results indicate that when the interface strength of soil- geotextile decrease by 22% (MRF= 0.78) as a result of wetting, the load bearing capacity of the embankment decreases by 30% as compared to the model constructed at OMC-2%.

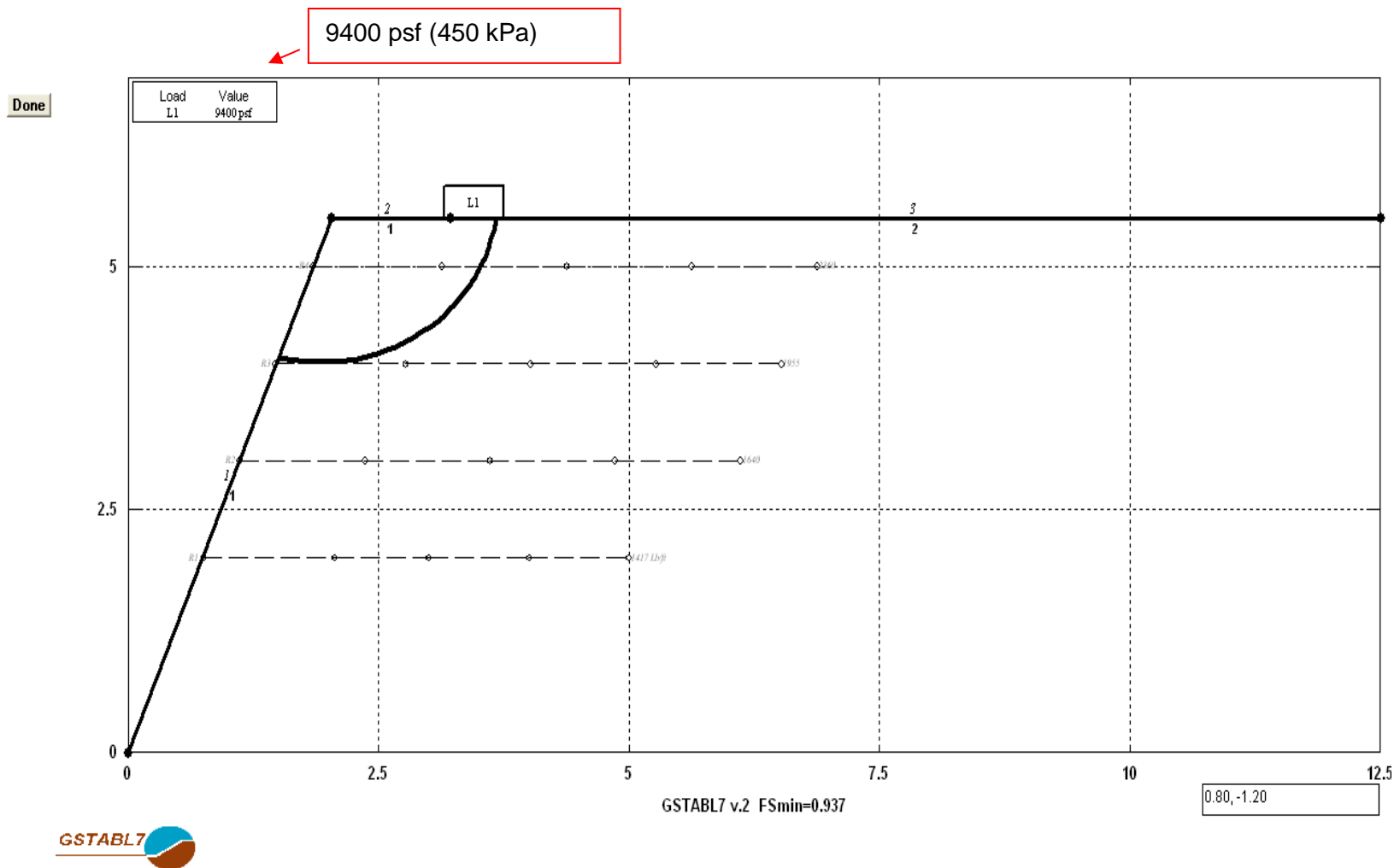Figure 36. Predicted slip plane and factor of safety for the embankment model constructed at OMC+2% from GSTABL analysis
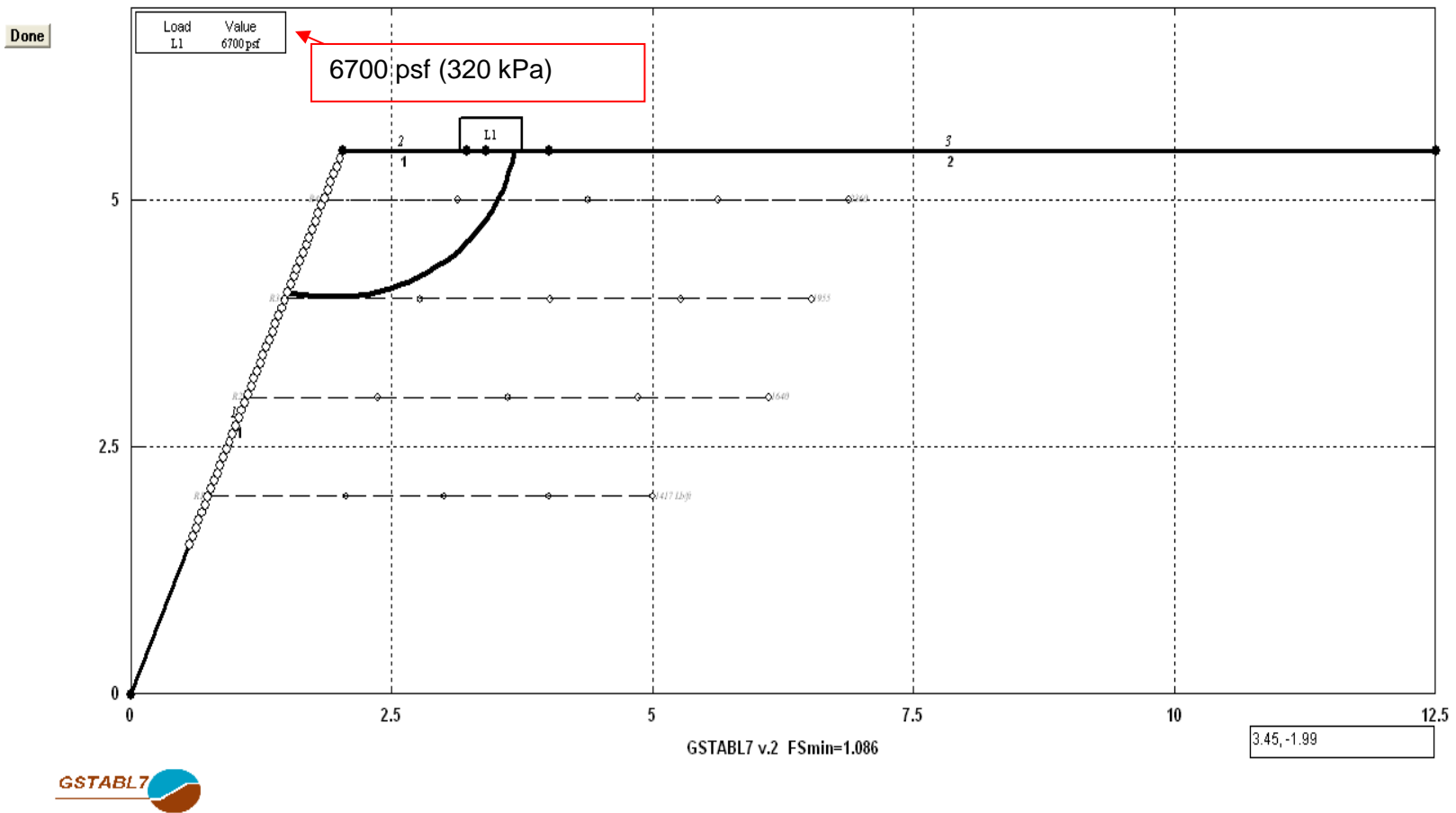
Figure 37. Predicted slip plane and failure load for the embankment model constructed at OMC+2% from GSTABL analysis to reach the factor of safety equal to 1.086. Note: White circles on the facing slope indicate the initiation points of possible slip planes formed within the large-scale embankment in GSTABL model.

7. MOISTURE REDUCTION FACTOR, $\mu(\omega)$

Figure 38 summarizes the μ(ω) values (i.e. MRF) for the reduced-scale indoor embankment tests as calculated from Equation 8:

$$\mu(\omega) = \frac{[(c_a + \sigma'_n \tan\delta)L_{IS}]_{for\ each\ test\ case}}{[(c_a + \sigma'_n \tan\delta)L_{IS}]_{at\ OMC-2\%}} \tag{8}$$

where L_{IS} is the length of the sheared soil-reinforcement interface and c_a and δ are interface shear strength parameters.

Figure 38. Moisture reduction factors from indoor embankment tests with HP370 and HP570 geotextile reinforcement

Results shown in Figure 38 for the indoor model embankments indicate that the moisture reduction factors [MRF or $\mu(\omega)$] for a change in the soil GWC value from OMC-2% to OMC+2% is approximately 74% in the case of HP370 geotextile reinforcement and 79% in the case of HP570.

8.   CONCLUSIONS

The primary objective of this study was to determine moisture reduction factors [MRF or $\mu(\omega)$] for the interface shear strengt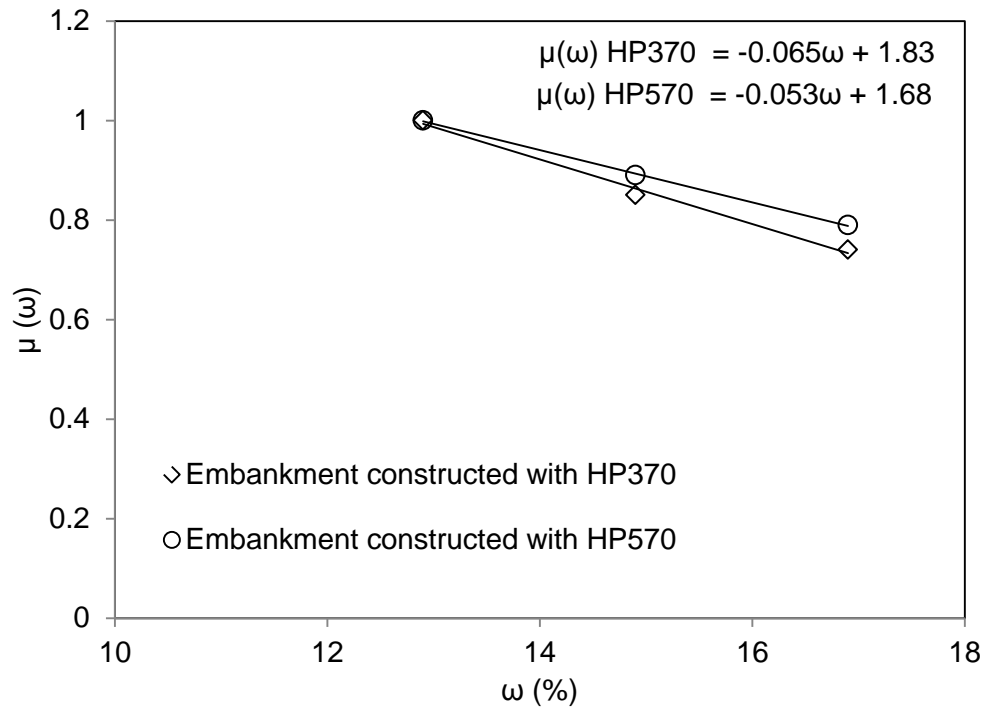h of geotextile reinforcement for the design of reinforced soil structures with marginal soils using multi-scale laboratory embankment tests. Based on the results of this study, the current FHWA equation for the shear resistance of soil-geotextile reinforcement interface could be modified to explicitly account for the influence of the unsaturated soil moisture content in the internal stability calculations of reinforced soil structures with marginal soils. The MRF values can help design engineers estimate the magnitude of reduction that could be expected in the soil-reinforcement interface shear strength as a result of wetting during construction or service life of the embankment structure.

The results of embankment tests in this study indicated that regardless of the size of the model examined, the embankment model constructed at OMC-2% resulted in the largest failure load when subjected to a line surcharge load simulating loading from bridge abutments. The failure loads of reduced-scale indoor embankment models that were built and tested at OMC+2% were as much as 40% smaller than that of the model compacted and tested at OMC-2%. The results of stability analysis using GSTABL also indicated that the bearing capacity of outdoor embankment model constructed at OMC-2% was 40% larger compared to the model at OMC-2%. The MRF values for the case of OMC+2% (using the OMC-2% case as baseline) for the embankment models constructed with HP370 and HP570 geotextiles were 74% and 79%, respectively.

9.   REFERENCES

ASTM International, 2008, "Standard Test Method for Density and Unit Weight of Soil in Place by the Rubber Balloon Method", American Society for Testing and Materials, West Conshohocken, PA, USA.

ASTM International, 2009, "Standard Test Method for Tensile Properties of Geotextiles by the Wide-Width Strip Method", American Society for Testing and Materials, West Conshohochen, PA, USA.

ASTM International, 2010, "Standard Test Method for Laboratory Determination of Water (Moisture) Content of Soil and Rock by Mass", American Society for Testing and Materials, West Conshohochen, PA, USA.

ASTM D4751, 2012, "Standard Test Method for Determining Apparent Opening Size of Geotextile", American Society for Testing and Materials, West Conshohochen, PA, USA.

ASTM International, 2013, "Standard Test Method for Determining the Shear Strength of Soil-Geosynthetic and Geosynthetic-Geosynthetic Interfaces by Direct Shear", American Society for Testing and Materials, West Conshohocken, PA, USA.

ASTM D4833, 2013, "Standard Test Method for Index Puncture Resistance of Geomembranes and Related Products", American Society for Testing and Materials, West Conshohochen, PA, USA.

ASTM D4632, 2013, "Standard Test Method for Grab Breaking Load and Elongation of Geotextiles", American Society for Testing and Materials, West Conshohochen, PA, USA.

ASTM D4491, 2014, "Standard Test Method for Water Permeability of Geotextiles by Permittivity", American Society for Testing and Materials, West Conshohochen, PA, USA.

Bathurst, R. J., Blatz, J. A. and Burger, M. H., 2003, "Performance of Instrumented Large-Scale Unreinforced and Reinforced Embankments Loaded by a Strip Footing to Failure", Canadian Geotechnical Journal, Vol. 40, No. 6, pp. 1067-1083.

Berg, R.B., Christopher, B.R. and Naresh C. Samtani, 2009, "Design and Construction of Mechanically Stabilized Earth Wallsand Reinforced Soil Slopes", Federal Highway Administration, Washington, DC, USA,FHWA-NHI-10-024.

Bilgin, O., and Kim, H., 2010, "Effect of Soil Properties and Reinforcement Length on Mechanically Stabilized Wall Deformations", Earth Retention Conference, ASCE, Bellevue, Washington, USA, pp. 556-563.

Boussinesq, J., 1885, "Applications des Potentials a lí Etude de lí Euilibre et Mouvement des Solides Elastiques", Gauthier-Villard, Paris.

Budhu, M., 2000, "Soil Mechanics and Foundations", John Wiley & Sons, Inc.

Bueno, B. S., Benjamim, C. V. S. and Zornberg, J. G., 2005, "Field Performance of a Full-Scale Retaining Wall Reinforced with Non-Woven Geotextile", Slopes and Retaining Structures Under Seismic and Static Conditions, ASCE, Geotechnical Special Publication No. 140, Gabr, Bowders, Elton, and Zornberg, Editors, Austin, Texas, pp. 2617-2625.

Chan, E., 2014. Reduced-Scale Laboratory Investigation of Reinforced Embankments. M.Sc. Thesis, The University of Oklahoma

Elias, V., Christopher, B.R. and Berg, R.R., 2001, "Mechanically Stabilized Earth Walls and Reinforced Soil Slopes-Design and Construction Guidelines", Federal Highway Administration, Washington, DC, USA, FHWA-NHI-00-043.

Esmaili, D., 2014. A Study on Unsaturated Soil-Geotextile Interface Strength Using Multi-Scale Laboratory Tests. PhD Dissertation, The University of Oklahoma

Esmaili, D., Hatami, K., and Miller, G.A., 2014, "Influence of Matric Suction on Geotextile Reinforcement Marginal Soil Interface Strength", Geotextiles and Geomembranes, 42(2): 139-153.

Fredlund, D.G., Morgenstern, N.R., and Widger, R.A., 1978, "The Shear Strength of Unsaturated Soils", Canadian Geotechnical Journal, Vol. 15, No. 3, pp. 313-321.

Gill, K.S., Choudhary, A.K., Jha, J.N., and Shukla, S.K., 2013, "Large Model Footing Load Test on Multi Layer Reinforced Coal-Ash Slope", Geo-Congress 2013, ASCE, San Diego, CA, pp. 489-498.

Gregory Geotechnical Software, 2003, GSTABLE, Version 2.0, Oklahoma City, OK.

Hatami, K., Garcia L.M. and Miller, G.A., 2010a, "Influence of moisture content on the pullout capacity of geotextile reinforcement in marginal soils", 61st Highway Geology Symposium, Oklahoma City, OK.

Hatami, K., Miller G.A., and Garcia L., 2010b, "Use of MSE Technology to Stabilize Highway Embankments and Slopes in Oklahoma", Oklahoma Department of Transportation, Tulsa, OK, USA, Final Report OTC REOS7-1-19.

Hatami, K., Garcia L.M. and Miller G.A., 2011a, "A Moisture Reduction Factor for Pullout Resistance of Geotextile Reinforcement in Marginal Soils", Geo-Frontiers, Dallas, TX, ASCE Special Publication No. 211.

Hatami, K., Miller G.A., and Esmaili D., 2011b, "Use of MSE Technology to Stabilize Highway Embankments and Slopes in Oklahoma", Oklahoma Department of Transportation, Oklahoma City, OK, USA, Final Report FHWA-11-04, ODOT SPR Item 2214.

Hatami, K., Miller G.A., Esmaili D., and Chan E., 2013, "Prototype Reinforced Soil Embankment for Reconstruction of US Route 62 Slope Failure in Chickasha, OK", Oklahoma Department of Transportation, Oklahoma City, OK, USA, Final Report OTCREOS 11.1-26.

Hatami, K., Esmaili D., Chan E., and Miller, G.A., 2014, "Laboratory Performance of reduced-Scale Reinforced Embankments at Different Moisture Contents", International Journal of Geotechnical Engineering, Vol. 8, No. 3, pp. 260-276.

Hossain, MZ., and Sakai, T., 2007, "A Study on Pullout Behavior of Reinforcement Due to Variation of Water Content of Soil", International Commission of Agricultural Engineering: CIGR E-Journal, Manuscript LW 07 011, Vol. 9.

Kawamura, S., Miura, S., Yokohama, S., Kudo, A., and Kaiya, N., 2013, "Field Monitoring of Embankment Constructed by Volcanic Soil and Its Evaluation", Geo-Congress 2013, ASCE, San Diego, CA, pp. 373-382.

Keller, G.R., 1995, "Experiences with Mechanically Stabilized Structures and Native Soil Backfill", Transportation Research Record, 1474: 30-38.

Keskin, M.S., and Laman, M., 2013, "Model Studies of Bearing Capacity of Strip Footing on Sand Slope", KSCE Journal of Civil Engineering, Vol. 17, No. 4, pp.699-711.

Kibria, G., Hossain, S., and Sadik Khan, M., 2014, "Influence of Soil Reinforcement on Horizontal Displacement of MSE Wall", International Journal of Geomechanics, ASCE, Vol. 14, pp. 130-141.

Kim, Y.T, and Lee, J.S., 2013, "Slope Stability Characteristic of Unsaturated Weathered Granite Soil in Korea Considering Antecedent Rainfall", Geo-Congress 2013, ASCE, San Diego, CA, pp. 394-401.

Kumar, A., Ohri, M. L. and, Bansal, R. K., 2007, "Bearing Capacity Tests of Strip Footings on Reinforced Layered Soil", Geotechnical and Geological Engineering Journal, Springer, Vol. 25, No. 2, pp. 139-150.

Miller, G.A. and Hamid, T.B., 2005, "Direct Shear Testing of Interfaces in Unsaturated Soil", Proceedings of EXPERUS, International Symposium on Advances in Experimental Unsaturated Soil Mechanics, Trento, Italy.

Ou, F.L., Cox, W. and Collett, L., 1982, "Rock Aggregate Management Planning for Energy Conversation: Optimization methodology", Transportation Research Record, 872: 63-69.

Riccio, M., Ehrlich, M. and Dias, D., 2014, "Field Monitoring and Analyses of the Response of a Block-Faced Geogrid Wall Using Fine-Grained Tropical Soils", Geotextiles and Geomembranes, Vol. 42, pp. 127-138.

Sawwaf, M. E. and Nazir, A., 2012, "Behavior of Eccentrically Loaded Small-Scale Ring Footings Resting on Reinforced Layered Soil", Journal of Geotechnical and Geoenvironmental Engineering, ASCE, Vol. 138, No. 3, pp. 376-384.

Yang, G.Q., Liu, H., Zhou, Y.T., and Xiong, B.L., 2014, "Post-Construction Performance of a Two-Tiered Geogrid Reinforced Soil Wall Backfilled with Soil-Rock Mixture", Geotextiles and Geomembranes, Vol. 42, pp. 91-97.

Yoo, C., 2013, "Effect of Rainfall on Performance of Geosynthetic Reinforced Soil Wall using Stress-Pore Pressure Coupled Analysis ", Geo-Congress 2013, ASCE, San Diego, CA , pp. 566-573.

Yoo, H., Kim, H., and Jeon, H., 2007, "Evaluation of Pullout and Drainage Properties of Geosynthetic Reinforcements in Weathered Granite Backfill Soils", Fiber and Polymers, Vol. 8, pp. 635-641.

Zhan, T.L.T., Ng, C.W.W., and Fredlund, D.G., 2006, "Instrumentation of an Unsaturated Expansive Soil Slope", Canadian Geotechnical Journal, Vol. 44, pp. 392-408.

Zhang, Z., Farrag, K., and Morvant, M. J., 2003, "Evaluation of the Effect of Synthetic Fibers and Non-Woven Geotextile Reinforcement on the Stability of Heavy Clay Embankment", Louisiana Department of Transportation and Development and Louisiana Transportation Research Center, Baton Rouge, LA, USA, Final Report LTRC 736-99-0760.